Molecular Dynamics Simulations on Crack Growth Behavior of BCC Fe under Variable Pressure Fluctuations

by

Xiao Xing

A thesis submitted in partial fulfillment of the requirements for the degree of

Doctor of Philosophy

in

Materials Engineering

Department of Chemical and Materials Engineering

University of Alberta

Abstract

Hydrogen embrittlement is an industrial problem involving in environment, loading mode, materials. Clarifying the mechanisms of hydrogen embrittlement not only makes economic sense but also academic significance. Although laboratory tests have gained significant understanding in the research of stress corrosion cracking (SCC), there are still limitations to study the effects of diffusible-atomic hydrogen on cracking. To get insights into nano-scale problem, such as the initiation of the micro-cracks, molecular dynamics (MD) simulation could be a good choice. There are some obstacles in applying MD simulations to field operations. Firstly, the current MD model is in nano-scale, however, the classical cracking mechanism is related to micro or centimeter scale plastic zone; secondly, former theoretical models only consider hydrogen movement during loading but ignore its movement during unloading. To bridge the nano-scale simulations with field operations, we are aiming to build a new model, i.e., the hydrogen atoms will diffuse out or accumulate into the plastic zone based on the stress intensity and hydrogen concentration gradient. In particular, an annulus region outside the plastic zone in bcc structure offers or depletes the hydrogen atoms to the plastic zone. Based on this hypothesis and the simulated results, the model could be used to predict the crack growth rate in different loading spectra.

To study the crack growth mechanism, we simplify our model to a nano-bcc structure plate, where the crack is located at one side of the plate or at the center of the loading direction. The static single loading is applied on the models with different concentration

of hydrogen. By tracing the hydrogen concentration in a nano region ahead of the crack tip, we found that the atomic ratio of H/Fe would reach 0.4 as ductile to brittle (DTB) transition happens. The total number of hydrogen atoms to saturate the plastic zone can be assessed with this critical hydrogen concentration. In addition, the asymmetric hydrogen diffusion in minor cycles could be quantified in our new model.

In addition, cyclic loading was applied to those models. The purpose of simulations is to detect the discontinuous crack propagation process. In MD simulations, hydrogen atoms do not diffuse out during unloading and consequently, form hydrogen-rich region ahead of crack tip. The hydrogen rich region blocks the dislocation emission and enhances the brittle cleavage of crack. The crack will propagate during both loading and unloading. However, as the crack pass through the hydrogen-rich region, the crack will become dormant. Several cycles of loading will then accumulate hydrogen atoms form new hydrogen rich region and brittle the crack, again. Moreover, we found the number of hydrogen atoms accumulated at the crack tip is also linearly related to the number of minor cycles. In addition, the linear accumulation mechanism could be applied to field operation and be used to predict the hydrogen accumulation acceleration effects.

This hydrogen-accumulation model had been used to predict critical loading frequency and could be further modified to predict the crack growth rate. The new model has offer a combined factor, which consider both stress intensity change and loading frequency change. The pH and temperature effects have been included in an environmental factor.

The new model has been used to predict crack growth rate in different loading spectra and steels and show good convergence. It is compared with previous combined factor and shows a power law relationship, which ensures its predictive capability.

Preface

Part of this thesis is involved in research collaboration:

Experiments in Chapter 3 (*Atomistic simulation of hydrogen-assisted ductile-to-brittle transition in α-iron*) were performed by Dr. Mengshan Yu and supervised by Dr. Weixing Chen in Department of Chemical and Materials Engineering, University of Alberta.

Experiments in Chapter 4 (*Atomics study of hydrogen embrittlement in cyclic loading: quantitative model of hydrogen accumulation effects*) were performed by Dr. Mengshan Yu and supervised by Dr. Weixing Chen in Department of Chemical and Materials Engineering, University of Alberta.

Experiments in Chapter 5 (*The effects of pressure fluctuations on hydrogen embrittlement in pipeline steels*) were performed by Dr. Mengshan Yu, and PhD Candidate Olayinka Tehinse, and supervised by Dr. Weixing Chen in Department of Chemical and Materials Engineering, University of Alberta; and Dr. J Been in NOVA Chemicals Corporation.

All other parts of this thesis are the original work of Xiao Xing.

Acknowledgments

First of all, my sincerest appreciation goes to my supervisor, Prof. Hao Zhang, for his extraordinary tolerance and patience, systematical guidance and continuous encouragement throughout my studies. I would also like to express many thanks to Dr. Weixing Chen and Dr. Reg Eadie for their valuable discussions. I acknowledge the members of the examining committee, Dr. Hao Zhang, Dr. Weixing Chen, Dr. Hyun-Joong Chung, Dr. Leijun Li, Dr. Chun-Wei Pao. Special thanks to examining committee chair Dr. Zukui Li.

I appreciate my colleagues, Miss Karina Chevil, Miss Zeynab Shirband, Miss Olayinka Tehinse and many others for their kind help during this research. I would especially like to thank Dr. Mengshan Yu, who was a Phd student and postdoctoral faculty member in our group, and Dr. Jiaxi Zhao who was a postdoctoral faculty member in our group for their patient mentoring at the beginning of my studies; and Mr. Devin Engel for his corrections of my writing tense and grammar in English.

I would like to thank the Natural Science and Engineering Research Council (NSERC), TransCanada Pipeline Limited, Spectra Energy, and the Pipeline Research Council International (PRCI) for financial support.

Last but not the least, special thanks go to my parents, Wensheng Xing and Lifeng Xing, for all they have done and continue to do for me; and my girl friend, Sichen Dong, for her love and tolerance throughout our past four years.

Table of contents

List of figures

Table

Nomenclature

NNpHSCC	Near Neutral pH Stress Corrosion Cracking
HEDE	Hydrogen Enhanced Decohesion
HELP	Hydrogen Enhanced Local Plasticity
HAC	Hydrogen Assisted Cracking
c_o	atomic hydrogen concentration
k_B	Boltzmann constant
Ω	partial volume of hydrogen atom
T	temperature
σ^{hyd}	hydrostatic stress
v	Poisson's ratio
σ_{ys}	yield strength
r_p	size of plastic zone
K_{max}, K_{min}, K_I	stress intensity (MPa*m$^{0.5}$)
R	K_{min}/K_{max}
R_{eq}	size of the annulus region which offers or depletes hydrogen atoms into plastic zone
P	stress field of the dislocation core
c_{eq}	equilibrium hydrogen concentration
r_o	the size of plastic zone which is generated by overloading
ϕ_{rH}	overloading retardation
G	shear modulus
μ	chemical potential

Chapter I Introduction

1.1 Hydrogen embrittlement and NNpHSCC

Hydrogen embrittlement was first observed when a piece of iron was immersed in acid and it lost toughness to bending test. And with lapse of time the metal slowly retain it's properties in breaking-strain [1]. A universal understanding is that hydrogen embrittlement is a reversible process in a small range of temperature and strain rate, which means, if the hydrogen atoms could be removed from the material, the material could retain its' properties.

Current research focuses on near neutral pH stress corrosion cracking (NNpHSCC) [2] in pipeline steel which is a process involved in both corrosion and fatigue [3][4]. Corrosion makes a contribution to crack growth and generate atomic H along with the cathodic reactions [5]. Fatigue not only enhances the crack propagation, but also generates cyclic fluctuations of stress intensity which creates hydrogen-charging condition. To study NNpHSCC, the hydrogen embrittlement mechanism is deserved to be clarified. Because hydrogen embrittlement in pipeline steel is a sever degradation mechanism involving in material, hydrogen charging condition and the loading [6][7] which has the same proposition with NNpHSCC. Despite decades of research, its mechanisms are still not fully understood and it continues to be a major threat to oil and gas transmission

pipelines worldwide. The pipeline failures cause significant economic loss, environmental pollution and/or casualties.

Revealing the hydrogen embrittlement mechanism needs multi-faceted knowledge, e.g., the hydrogen source, how hydrogen enters the base metal, diffuses through lattice or along the grain boundary, what type of microstructures can trap hydrogen atoms. Several mechanisms of hydrogen embrittlement in metals developed in the last several decades have been listed as follows.

1.1.1 Hydrogen enhanced decohesion (HEDE)

The hydrogen enhanced decohesion model proposed by Troiano and Oriani [8,9] suggests that the role of hydrogen is to weaken the inter-atomic bonds in the steel, thereby facilitating grain boundary separation or cleavage crack growth. It has the same implication with the surface energy theory proposed by Petch and Stables [10]. Figure 1.1 (a) show some small dispersed fracture planes with dotted line in a specimen without hydrogen, and fracture plane in specimen (b) is much larger than (a) because of the presence of hydrogen atoms [11]. The brittle failure is always inter-granular fracture, and this can be explained in terms of trapping of hydrogen atoms near grain boundaries or phase boundaries [12,13]. The HEDE is also related to stress intensity, because this process is dependent upon the activity of hydrogen dissolved in the metal lattice. A very high local tensile stress leads to nucleation of micro-cracks because of hydrogen accumulation [14]. In this way, the HEDE theory has some connections with hydrogen bubble theory [15,16].

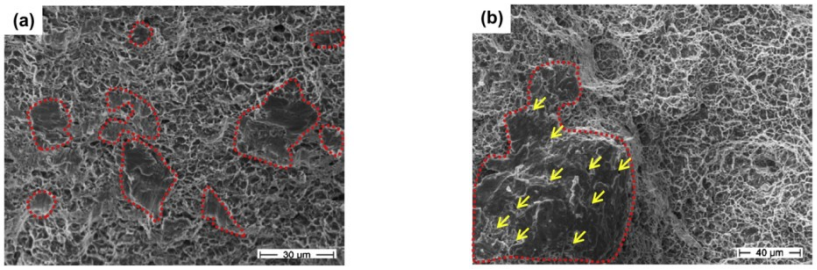

Figure 1.1 The fracture surface of broken steel under static loading.(a) is a sepcimen free of dissolved H atoms. (b) is a specimen charged with hydrogen atoms. [11]

1.1.2 Hydrogen enhanced local plasticity

Various researchers have suggested that hydrogen will reduce the critical stress for dislocation emission, thereby increasing the amount of plastic deformation near fracture surfaces. This theory is firstly proposed by Morgan and Mcmohan [17,18]. Lynch later found the same phenomenon and proposed that this process involved the facilitation of dislocation emission at crack tip [13,19].

This process is a highly localized plastic failure rather than an embrittlement[20,21]. Hence, one contradictory theory is that H atoms form Cottrell atmospheres, which generate solute drag and therefore resist the dislocation motion [22] as figure 1.2 shows. Some experimental results can support this theory that the specimen free of hydrogen charged has wide-spread and dense slip bands compared with hydrogen supercharged specimen as figure 1.3 has shown. However, the HELP mechanism is supported as one of the embrittlement mechanisms. Because dislocations will increase the strain energy near the grain boundaries where they incorporated and make the inter-granular failure much likely to happen [23].

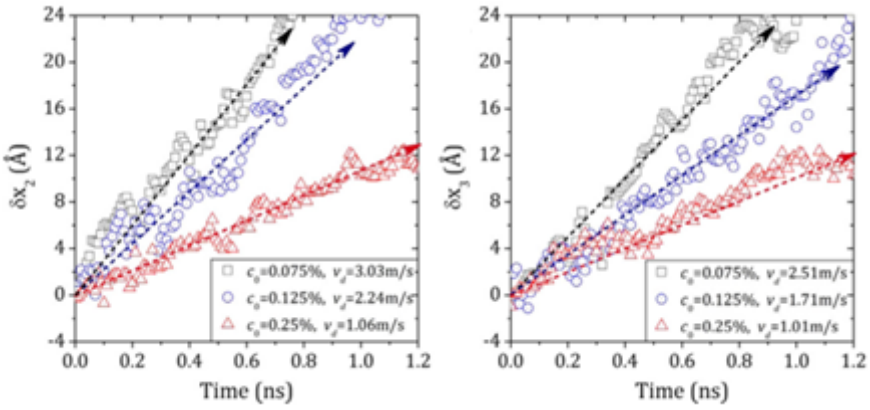

Figure 1.2 Time evolution of the x coordinate for dislocation cores after the application of stress 400 MPa. The velocity of dislocations decreases as hydrogen concentration is increased. [22]

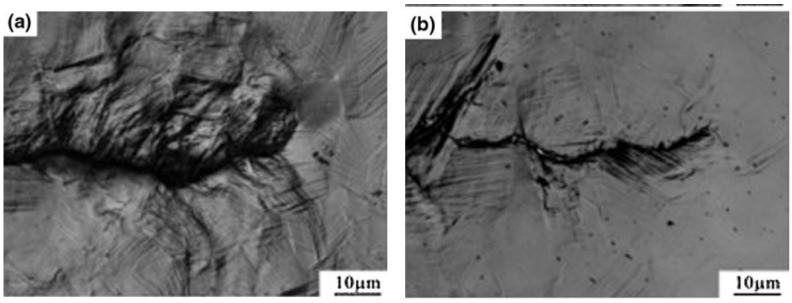

Figure 1.3 Slip deformation behavior near fatigue crack tip in type 304 steel. (a) uncharged specimen with C_H=2.2 wt ppm.(b) C_H=47.2 wt ppm. 2a=3mm,σ=280 MPa. [23]

1.1.3 Hydride formation and cleavage

The nucleation of hydrides has been firstly observed in titanium alloy. It is postulated by Gahr [24], however, the hydrides are unstable and may dissolve quickly as the crack pass through them in steel [25]. This is a stress-intensity based mechanism. At low stress intensities, hydride formation decreases the local stress intensity at the crack tip and as a

result continued fracture need an increment in external stress. Once the local stress intensity is increased to exceed the stress intensity needed for hydride fracture, the crack can proceed by repeated hydride nucleation, growth and cleavage. At high stress intensities, the failure is by a constrained plastic mechanism in which the stress for plastic flow is reduced at a higher hydrogen concentration [24,25].

1.1.4 Hydrogen triggered ductile-to-brittle transition

This mechanism is based on large-scale molecular simulations, and developed by Curtin and his coworkers [22,26,27]. They postulated that hydrogen accumulation in a nano-size region around crack tip can constrain the dislocation slip bands and make the ductile to brittle transition happens. In Ni-H case, a nano-hydride can form[28], the model is built as Eq. [1.1] has shown. This equation can be used to predict the size of the nano-hydride under specific temperature T and time t. As the figure 1.4 has shown, this size of the nano-hydride is L and hydrogen atoms will move into this region and saturate it at atomic ratio 1.

$$\frac{\pi}{2}\left(L+R\right)^2-\frac{\pi}{2}R^2=2.1c_o\left(\frac{5(1+\upsilon)D\Omega\dot{I}}{12\sqrt{2\pi}k_BT}\iota\right) \qquad [1.1]$$

where R is the inner radius of crack tip as figure 1.4 has shown, c_o is the hydrogen concentration far away from crack tip, υ is Poisson's ratio, D is the diffusivity of hydrogen atom, Ω is the partial volume of hydrogen, $\dot{I}$ is the changing rate of stress intensity and k_B is the Boltzmann constant.

While in Fe, the mechanism is based on the stacking fault energy and free surface energy deduction[29]. Equation [1.2] can be used to predict the crack growth rate in brittle iron with high hydrogen concentration.

$$\dot{a} = \frac{4}{\pi}\frac{D\Omega}{k_B T}\frac{(1+\nu)K_I}{3\sqrt{2\pi}}\left(\frac{\pi c_o}{a_o}\right)^{5/4}\Delta a^{-1/4} \qquad [1.2]$$

Where $\dot{a}$ is the crack growth rate, a_o is the lattice parameter, and Δa is the crack length change. Both models are based on hydrogen diffusion and accumulation theory. Hydrogen movement assessment only involves in the stress intensity change, however, ignores the hydrogen concentration gradient. The difference is that, in Ni case, hydrogen atoms will saturate a nano-size annulus region; however, in Fe case, the hydrogen atoms are saturating two free surfaces at atomic ratio 1 ahead of the crack tip.

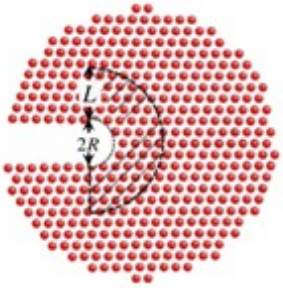

Figure 1.4 The geometry of the crack tip. R is the radius of the crack tip and L is the size of the annulus nano-hydride.[28]

Of these mechanisms, both HEDE and HELP can refer to the inter-granular cracking mechanism. Trapped hydrogen atoms along the grain boundary can weaken the metal bonds (HEDE) and incorporated dislocations will increase the strain energy (HELP). The DTB transition mechanism is related to the diffusible hydrogen atoms saturating free

surfaces ahead of crack tip, which could be related to trans-granular cracking mechanism. However, all of the mechanisms mentioned above have verified that the accumulated hydrogen atoms can enhance crack propagation. In current research, we should quantify the hydrogen accumulation rate under different pressure fluctuations (spectra) before quantifying the crack growth rate.

1.2 Current Experimental observations in NNpHSCC

The experimental work on X-65 and X-60 pipeline had shown corrosion would occur at the crack tip as well as on the crack walls; this would turn a crack characteristic of a sharp tip into a pit [3]. However in the near-neutral pH groundwater, some of the dormant cracks (about 5%) can grow continuously [30]. Several parallel experiments are conducted under cyclic load and using C2 and NOVATW as the solutions: the current understanding is that because of the higher dissolution rate, the hydrogen concentration is much higher in C2 solutions, and more hydrogen will enhance the crack re-sharpening process and help the crack grow continuously [4].

A mathematical model is built to predict crack growth rate based on former study and is shown as

$$(\frac{da}{dN})_{tot}=m[\frac{\Delta K^{\alpha}K_{max}^{\beta}}{f^{\gamma}}]\,(\frac{da}{dN})_{CF}+\mathrm{C(t)} \qquad [1.3]$$

where $\alpha+\beta=1$, Υ is a constant representing corrosiveness of the environment. ΔK is the stress intensity factor range, which can be related to the pressure fluctuation and the dimension of existing cracks in the pipeline; K_{max} is the maximum stress intensity factor corresponding to the maximum pressure and the crack dimension in a given pressure

cycle, *C(t)* is a crack depth (*t*) dependent function reflecting crack growth rate by corrosion dissolution[5,6].

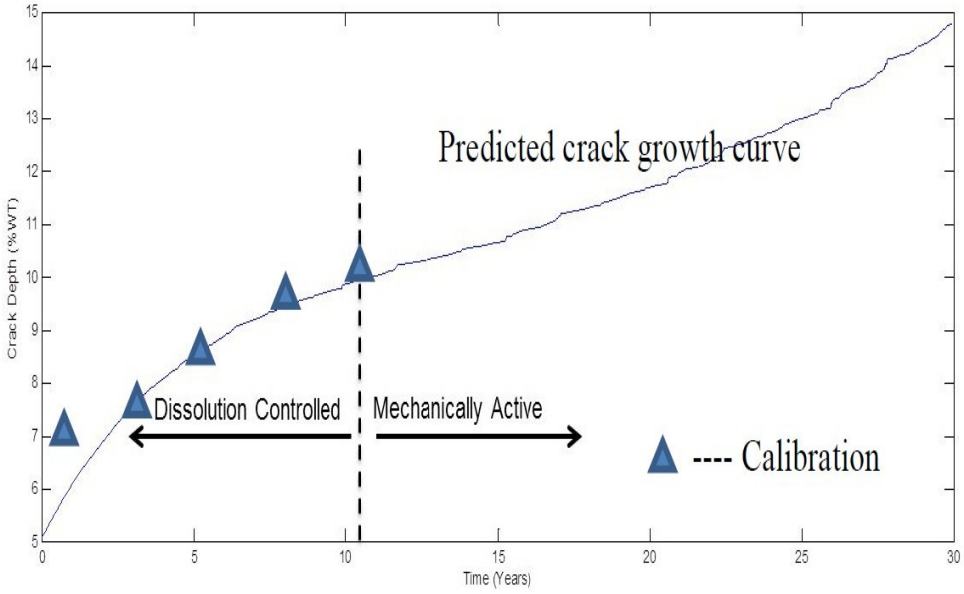

Figure 1.5 Example of predicted crack growth curve of a crack in X-65 pipeline steel with a wall thickness of 9.88 mm. (provided by Brett Conrad)

Figure 1.5 shows an example of predicted crack growth curve of a X-65 pipeline with a wall thickness of about 9.88 mm. The predicted accuracy will certainly depend on the accuracy of the input data. However, the use of a self calibration process as shown in the figure 1.8, can be applied to the predicted curve and seek the accurate values of those constants in Eq. [1.3]. After this initial calibration, the prediction can be revalidated in the future.

Currently, a series of experiments on X-60 pipeline are carried out to investigate the effect of cyclic loading, especially the unloading, on crack propagation. These

experiments not only focus on the frequency of under loading but also the minor cycles /hold between under loads. The outcomes suggest that minor cycles existing in underload spectra can enhance crack growth significantly, and hold sections in spectra can blunt the crack tip and hinder crack growth as Fig. 1.6 has shown.

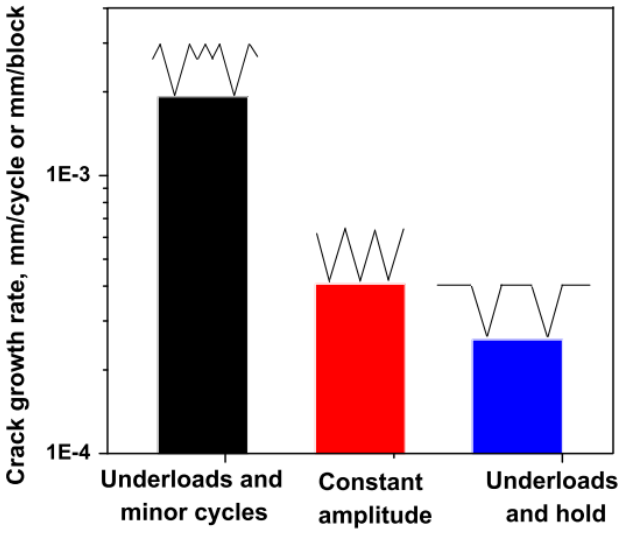

Figure 1.6 Comparison of crack growth rate in different waveforms to show the importance of minor cycles in enhancing crack growth. [31]

There is a critical loading frequency below which crack growth rate will remain constant and maximum. This phenomenon could be only detected in the hydrogen charged specimen and remind that it's related to hydrogen-enhanced crack growth mechanism as Figure 1.7 shown [32].

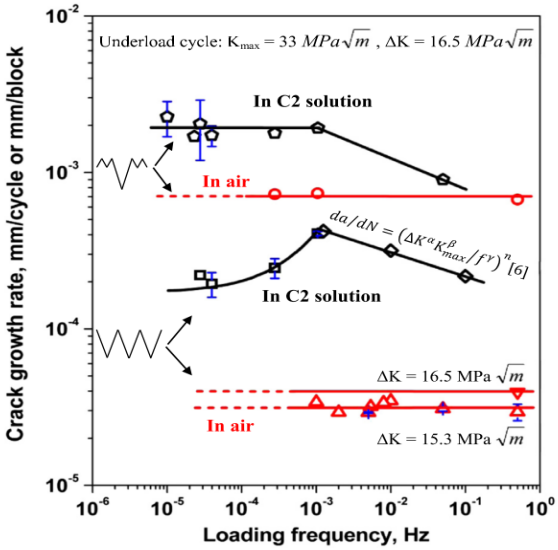

Figure 1.7 Comparison of crack growth rate under different loading frequency for constant amplitude and underload amplitude waveforms in air and in C2 solution. [32]

These results suggest that hydrogen accumulation and saturation affect the frequency – dependence crack growth. The crack growth model should be modified to a new form as Eq. [1.4] has shown, where the $\left(\frac{da}{dN}\right)_{HAC}$ is the hydrogen assisted cracking rate, which is related to loading stress intensity and environmental factors. As the loading frequency f reach f_{critical}, the hydrogen assisted cracking rate reach maximum.

$$\left(\frac{da}{dN}\right)_{tot} = \left(\frac{f_{critical}}{f}\right)^{\gamma} \left(\frac{da}{dN}\right)_{HAC}^{max} \qquad [1.4]$$

Current tests also suggests that using minor circles replacing the holding phase, the under loading phase will produce worse effect on pipeline. This effect has been shown in figure 1.6. And the minor cycles' acceleration effect is also verified in the figure 1.7.

Lots of laboratory tests in SCC group has shown the complexity of H effect in NNpHSCC. Figure 1.8 shows the competition between crack tip blunting and sharpening for pipeline in NNpHSCC under static load. Experimental works show that a pre-existed axial crack will remain dormant under static loading. Actually, mild mechanical cycling would also lead to crack dormancy. This outcome is consistent with the fact that 95% of crack population whose depth reach to 0.5 mm come to dormant state [7]. Figure 1.9 shows that a predominant factor causing these cracks to be blunt in NNpH environments do not cause pipeline steels to passivate, and general corrosion happens both at the crack tip and on the crack walls. Another factor which depends on the type of pipeline steels and prior loading history of the pipeline steels is low temperature creep (LTC)[8]. LTC will also happen at stressed crack tip.

Opposite to blunting process, crack sharpening can be achieved by developing micro-cracks ahead the crack tip when hydrogen segregates into the hydrostatic zone, which is highly deformed area ahead of the crack tip. This process is unlikely to occur under static loading and when crack depth is at least 1.0mm, the micro-cracks do not link up with main crack.

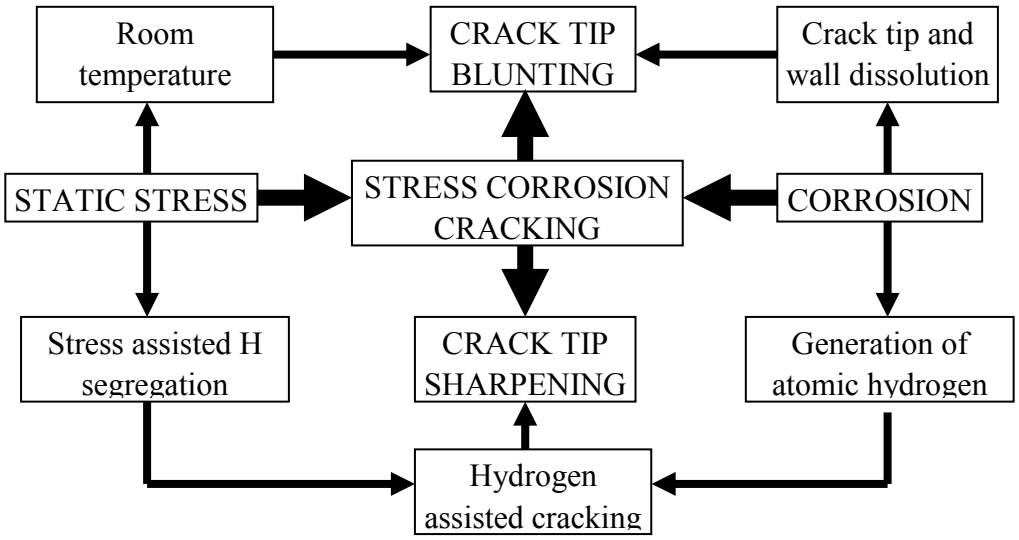

Figure 1.8 A schematic showing the competition between crack tip blunting and crack tip sharpening in the pipeline steels exposed to near neutral pH environments under constant loading stresses (situation of stress corrosion cracking). [12]

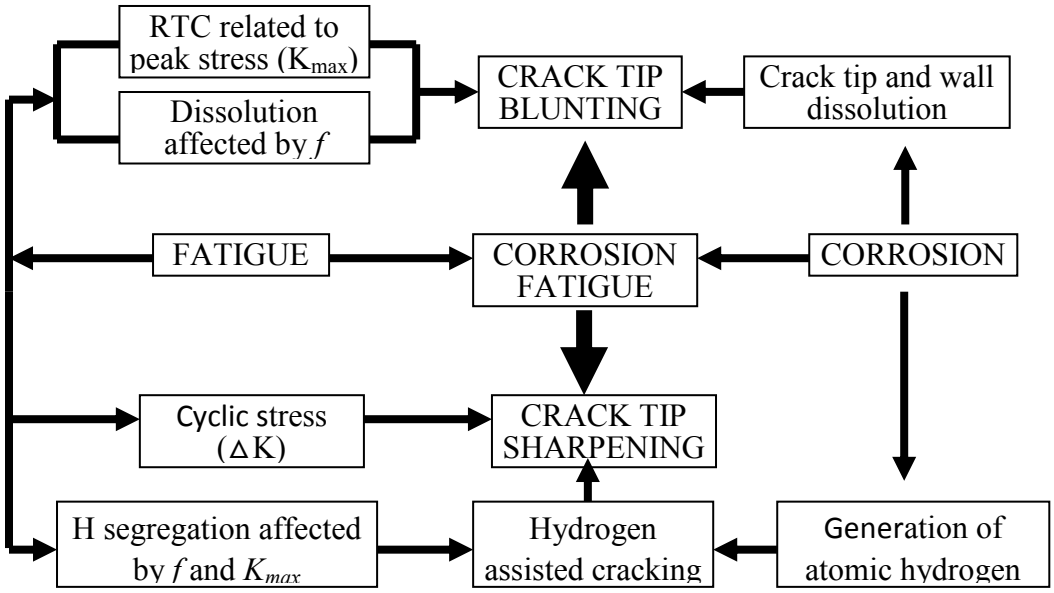

Figure 1.9 A schematic showing the competition between crack tip blunting and crack tip sharpening in the pipeline steels exposed to near neutral pH environments under cyclic loading condition (scenario of corrosion fatigue).[12]

When cyclic loading is applied, the blunting mechanisms as discussed previously are still applicable. The difference is that LTC increases with an increment of the applied stress and creep time. The analysis of the competitive process for blunting and sharpening under cyclic loading is shown in Figure 1.9.

From experimental observations, when determining the threshold $K^2K_{max}/f^{0.1}$ value for long cracks, above correlation will be true for shallow cracks expect that those were found growing at appreciable rates below the threshold of long cracks. In fact, the cracks

are more likely grow under cyclic load in NNpH environments is a phenomenon in the field of fatigue. However the fatigue will not be the sole reason as the dormant cracks representing 95% of total crack population [9]. Hydrogen related sharpening also exist under fatigue loading, even this sharpening mechanism is more influential under SCC loading compared with fatigue loading.

As a conclusion, the mechanism governing crack re-sharpening is an interaction of fatigue loading and H-related effect [10]. Hence, the crack growth rate could be related to the hydrogen diffusion rate near crack tip under NNpH condition. There are three available crack growth models listed below, which could be used as reference when we build a new one.

1.3 Available crack growth model in NNpHSCC

1.3.1 Paris law

As expressed by equation $\left(\frac{da}{dN}\right) = c\Delta K^m$, the Paris Law only considers one basic parameters of fatigue, i.e., the stress intensity factor range ΔK. It could well model the crack growth behavior in inert environments where K_{max} and loading frequency have insignificant influence. However, loading frequency does play an important role in the crack growth rate in NNpHSCC [12,32].

1.3.2 Superposition model

The superposition model applied in near-neutral pH environments is given as:

$$\left(\frac{da}{dN}\right)_{total} = \left(\frac{da}{dN}\right)_{fatigue} + \frac{1}{f}\left(\frac{da}{dt}\right)_{SCC} \quad [1.5]$$

where $(da/dN)_{total}$ is the total crack growth per cycle in a near-neutral pH solution, $(da/dN)_{fatigue}$ is the crack growth per cycle in air, f is the loading frequency, and $(da/dt)_{SCC}$ is the crack growth in terms of time in a near-neutral pH solution by SCC.

However, the crack growth of pipeline steels under static loading in near-neutral pH environments (NNpHSCC) has never been observed, except for the crack initiation resulting from galvanic corrosion [3][12][33]. On the other hand, the loading frequency in the field is very low, for example, typically about 10^{-5} Hz for high pressure gas transmission pipelines. As a result, 1/f would be very large and could be even larger than the fatigue term. As shown in figure 1.7, the inverse relationship between the crack growth rate and loading frequency at frequencies lower than 10^{-3} Hz overestimates the crack growth rate.

1.3.3 Combined factor

Based on long-term and extensive laboratory crack growth simulations under constant amplitude cyclic loading in near-neutral pH environments, it is found that the crack growth rate can be correlated to a combined factor that incorporates both the mechanical and the environmental driving forces [33][5]as:

$$\frac{da}{dN} = a\left(\frac{\Delta K^{\alpha} K_{max}^{\beta}}{f^{\gamma}}\right)^{n} + b \quad [1.6]$$

where *a, n, α, β,* and γ are all constants. $\left(\Delta K^{\alpha} K_{max}^{\beta} / f^{\gamma}\right)$ is termed as the combined factor. The relative contribution of ΔK and K_{max} to crack growth is represented by α and β, γ is a factor representing the influence of the corrosion environment on the crack growth rate, which is found to be around 0.1, b is the contribution of stress corrosion cracking, which was found to be about one order of magnitude lower than the first term in Stage II crack growth, and it can be ignored. ΔK and K_{max} are strongly dependent on the geometry of the specimen, while γ is dependent on the corrosiveness of the environment. A threshold value of $\left(\Delta K^{\alpha} K_{max}^{\beta} / f^{\gamma}\right)$ is also determined, below which the crack will cease to grow [33].

The combined factor model could correlate well with the constant amplitude fatigue crack growth rate of pipeline steels exposed to near-neutral pH environments. However, when it comes to the field pressure fluctuations, it may contradict the fact that failure of pipelines by cracking in the field can occur as soon as a few years after the surface. This phenomenon raises the possibility that certain loading interactions may enhance crack growth, and the crack growth model of different spectra should be developed separately.

1.4 The reasons to employ MD simulations

The mechanism for hydrogen embrittlement in atomic level cannot be directly detected in current available experimental technologies. Considering the urgent need in studying cracking mechanism and building theoretical model for H effect in growing crack, molecular dynamics (MD) simulation is a potentially good alternative choice.

MD simulation is a technique used to compute the equilibrium and transport properties of a classical many body system which follows Newton's equation of motion. MD could compute thermodynamics, atomic structural and kinetic properties; it also enables scientists to study the motion of individual atoms. MD originated from statistical method of studying large number of particles by Maxwell and Boltzmann [34], and is firstly introduced to ensemble hard spheres by Alder and Wainwright [35]. Real materials MD simulation was first conducted by Gibson et al. in analyzing copper's radiation damage [36]. Rahman was the first to employ realistic potential in simulating liquid argon [37]. The advantages of employing this method to study cracking mechanism have been listed as follows.

1. Interatomic potential function for describing materials and the atomic positions with initial velocity are the only input required by MD simulation. And MD method enables exact temperature, pressure control which ensures that it can completely rule out the human errors in experiments.
2. MD simulation enables an investigation in small spatial scale (nano-meter) and time scale (nano-second).
3. Compared with experimental tests, MD simulation requires much lower cost.

Despite of all advantages brought by MD, there are limitations to this method. MD simulations can be only carried on nano-level spatial and time scale, however, the rupture

of a crack may take several years; the strain rate is many orders higher than that applied in laboratory tests, therefore, the stress intensity near the crack tip cannot even be released during unloading simulations; It is impossible to simulate entire plastic zone using MD simulation. In conclusion, MD and experimental method can mutual complementary.

1.5 Current outcomes of MD simulations in Fe-H and Ni-H systems

In this section, we will review some of the previous MD simulations in Fe-H and Ni-H systems.

The hydrogen assisted crack growth process in steel could be simplified to crack growth in a typical body center cubic model. To introduce hydrogen atoms into the metal, the type of interstitial sites where the hydrogen atoms can stably stay should be determined, firstly. Hydrogen atoms will stably stay in tetrahedral sites in Fe and stay in octahedral sites in Ni [38][39]. Introducing the hydrogen atoms into the model should follow the stress distribution with the equation listed below [40]. The grain boundaries will trap hydrogen atoms because of extra volume [41,42] and the dislocation core will bring in extra stress to trap hydrogen atoms [43–45], too. These retardation factors for hydrogen diffusion will be only considered in specific simulations.

$$c_{eq} = c_o \exp\left(\frac{\sigma^{hyd}\Omega_H}{k_B T}\right) \qquad [1.7]$$

The fracture mode in atomic simulation show orientations' based mechanism, hence poly-crystal model is needed in studying phase transformation at crack tip in

nanocrystalline Fe, where the model is created using Voronoi construction [46]. In this construction, the crystals are randomly nucleated in a cubic, and the construction of the boundary structure is similar to what is expected in polycrystalline material. It was found that plastic deformations near the crack tip are not associated with dislocation emission, but phase transformation and grain nucleation. At the crack tip, stress is released by bcc1 to fcc phase transformation and further released by fcc change back to different orientation bcc [47].

Our previous simulations have revealed the hydrogen induced softening/hardening effect in single α-iron under uniaxial tensile loading. The model was created with a dimension 5×20×26 nm and oriented in directions [1 0 0], [0 1 0], [0 0 1] respectively, in which the [0 0 1] direction was the loading direction. Hydrogen concentration, temperature and vacancies near dislocation core are the factors affecting the hydrogen induced hardening effect and three conclusions could be listed as follows: 1) the hydrogen pinning effect lead to yield strength increasing as hydrogen concentration is increased; 2) de-association of hydrogen from dislocations is related to the breaking of binding between hydrogen atoms and dislocations; and 3) the vacancies could enhance Fe-H bond at the expense of the exiting of Fe-Fe bond, which leads to decohesion [19]. The figure 1.10 illustrates the first two conclusions.

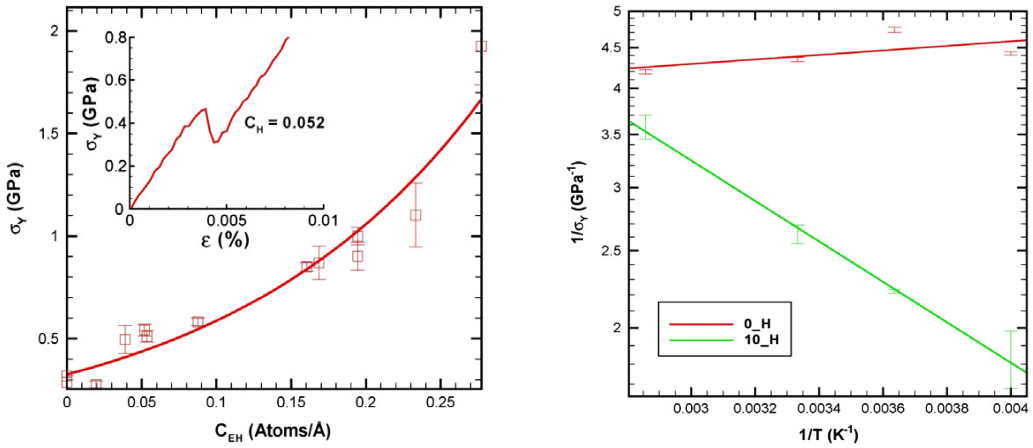

(a) (b)

Figure 1.10 (a) Yield strength as function of effective hydrogen concentration in dislocation. A typical stress strain curve is shown in the inset. (b) Yield strength as a function of temperature in the cases of hydrogen free and 10 hydrogen atoms. [19]

Hydrogen diffusivity was previously determined in bulk, on surface, or in symmetry grain boundary [48]. The higher activation energy will induce higher barrier for hydrogen to cross and continue the diffusion process; hence the grain boundary has the trapping sites for hydrogen. Another significance of this research is quantifying the hydrogen diffusion in bulk with the hydrostatic pressures which is shown in Fig. 1.11 and confirms that the difference in diffusivity due to the pressure change could be as large as two orders of magnitude. This conclusion helps to calibrate the diffusivity we use in the future model. The corrected diffusivity according to experimental tests is shown as $D=1.585*10^{-8}*EXP(-5567.38/8.314/T)$ [49,50].

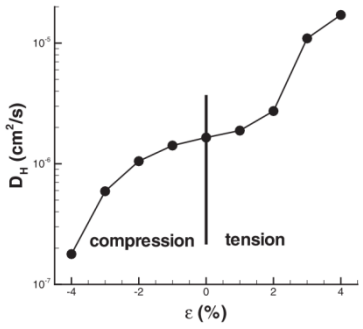

Figure1.11 Diffusion coefficients of hydrogen atoms as a function of hydrostatic pressure in the bulk Fe. [48]

Pre-charge and dynamical charge methods in Ni-H system [20] show that for H precharged system, the structure relaxed with a predetermined concentration. While for dynamically charged system, H was introduced at a desired strain load and diffused according to the new stress field. In most MD simulations, the dynamically charged method is used because Chang and Hirth showed that for spheroidised AISI steel [21], the precharged specimen exhibited ductile failure and the dynamically charged specimen exhibited failed in brittle fracture.

Curtin and his co-workers' work has been described in the 1.1.4 section and the details of their DTB theory are elaborated here. In Fe-H system, hydrogen embrittlement effect could be summarized in two key parameters, K_I^c and K_I^e [51]. Two models with different orientations (crack plane normal) [crack front direction] of (111) $[11\bar{2}]$ (orientation I) and (111) $[1\bar{1}0]$ (orientation II) which had dimensions Lx×Ly×Lz of 485 Å×480Å×24Å and 480 Å×485Å×28Å are studied, respectively. The system is firstly deformed to a constant

load, then hydrogen atoms are introduced into the tetrahedral sites randomly near the crack tip at a rate 1 atom per picoseconds. Applying mode I load on the two ends of loading direction, and the conclusion is that hydrogen decreasing the K_I^c faster than K_I^e which make the material change from ductile to brittle. Hydrogen atoms form a stress concentrated region near crack tip and block the path of dislocation emission which made the crack become cleavage.

A parameter A_0 is provided to judge whether the crack is cleavage or ductile as the Eq. [1.8] shows,

$$N_H/L_z=A_0K_I^{8/5};\ A_0=\beta\left(\frac{1}{2,}\frac{9}{10}\right)\frac{2c_0}{a_0^3}\left(\frac{5(1+v)D\Omega}{12\sqrt{2\pi}k_BT\dot{K}_I}\right)^{4/5} \quad [1.8]$$

Where β is the beta function and a_0 is the lattice constant, v is Poisson's ratio, T is temperature, Ω is partial volume of an H interstitial in Fe and c is the concentration of H. A_0 is the single overall parameter that controls the kinetics of H aggregation at the crack due to any combination of loading, diffusion, concentration and temperature. And For any value of A_0, Eq. [1.8] predicts the evolution of N_H/Lz as a function of the value of K_I. There is a critical value for A_0 which divides the material response into ductile (dislocation emission) and brittle (cleavage) domains, as shown in Fig. 1.12 [22].

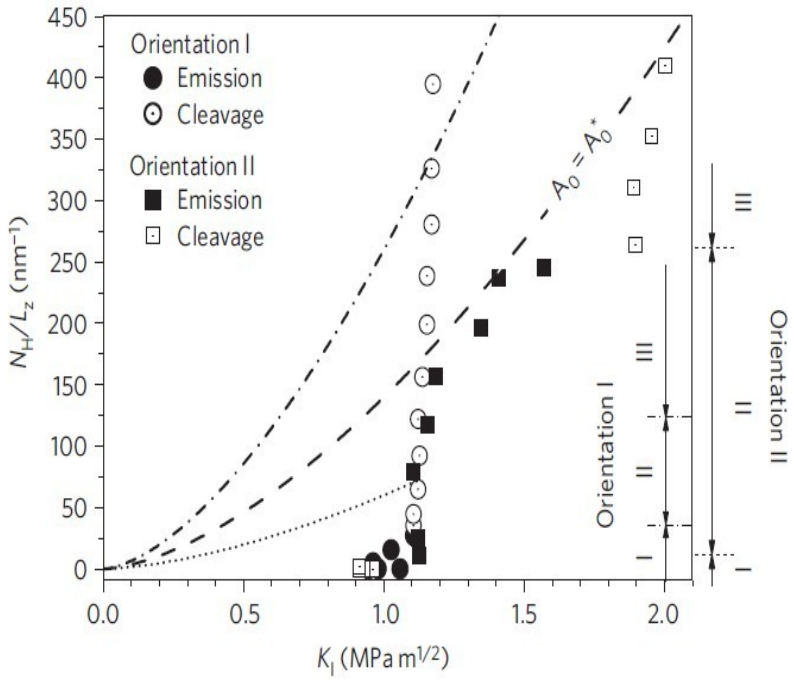

Figure 1.12 The amount of H in the system normalized along the crack line direction, N_H/Lz, versus the stress intensity K_I at which either dislocation emission or brittle cleavage occurs, as found in simulations for orientations I and II. [22]

After the brittle cleavage model is built, they continue to study the motion/mobility of dislocations and the structure of edge dislocation pile-ups in Fe in the absence and presence of dissolved H [22]. A total number of H atoms trapped in an edge dislocation core has been quantified as,

$$N_H(c_o) = Z_o \int_0^{2\pi} \int_0^R \left[\frac{c_o \exp\left(\frac{p\Omega}{k_B T}\right)}{1 + c_o \exp\left(\frac{p\Omega}{k_B T}\right)} - c_o \right] r dr d\theta \qquad [1.9]$$

where p is stress distribution in the dislocation core. This calculation helps to quantify how many hydrogen atoms should be introduced into the model. The conclusion is that H atoms cause solute drag, therefore resisting rather than facilitating dislocation motion. In addition, hydrogen atmosphere provides no shielding of dislocation interactions.

MD simulations can not only simulate single static loading, but also simulate complex cyclic loading. The loading mode of MD simulations in direction [0 1 0] (1 0 1) is shown in figure 1.13 (a), after applying 12 rectangular cyclic loadings on the model, there was a phase transformation from bcc to hcp is observed during unloading portion [52]. As the dislocations reach grain boundaries, these dislocations began to pile up, and phase transformation disappear. During the unloading process, the emitted dislocations would move back to the crack tip. After twelve repeating loading processes, they observed that cyclic loading not only generates several vacancies around the crack tip because of un-reversible plastic dislocations, but also enhance the propagation of the crack. The cyclic loading on orientations $\langle 11\bar{2}\rangle(111)$ and $\langle 00\bar{1}\rangle(110)$ induce brittle cleavage and twinning and slip bands were observed during crack propagation [53]. The cracks propagation mechanisms are orientational dependent, and the type of grain boundaries have different effects on crack growth. In simulations, $\Sigma 3$ grain boundary has no effect on blocking crack growth. However, $\Sigma 5$ grain boundary has an effect on releasing strain hardening and hindering crack propagation.

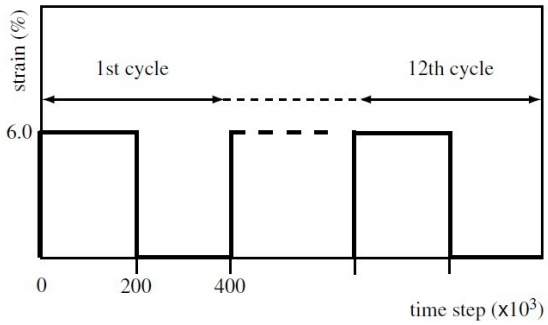

(a) loading pattern subjected to the system orientation

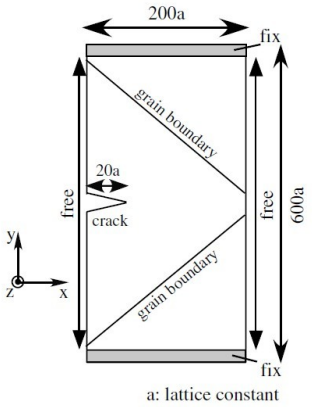

(b) the crack model in [0 1 0] (0 0 1)

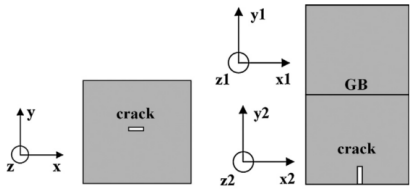

(c) the typical model in $\langle 00\bar{1} \rangle (110)$ and $\langle 11\bar{2} \rangle (111)$ and in $\Sigma 3$ or $\Sigma 5$ grain boundaries.

Figure 1.13 The sketches of the cracks and the loading modes. [52,53]

MD simulations in Fe alloy which contains Cr, Ni, and hydrogen atoms report the energy of metal bonds and metal-H bonds is a key factor to brittle cleavage. It suggests that hydrogen embrittlement is strongly affected by grain boundary structure. The boundary lacking of gaps and structural irregularities have better resistant to embrittlement. This theory could be related to crack tip simulation near poly-crystal grain boundary. Another explanation to the HEDE theory is that the electrons transferred to the H atoms from metal helped to form the new H- metal bonds and conversely decrease the metallic bonds near H atoms [26].

1.6 Outstanding questions

As experiments and simulations have shown, fracture modes are based on the orientations of cracks. The fracture mechanism for each orientation should be summarized separately. Loading interactions also has a significance effect on crack growth. Hence, as movement velocity of hydrogen atoms in steel has been quantified, a crack growth model to predict hydrogen enhancement in cyclic loading should be developed. Below are the outstanding questions yet to be answered.

1.1 How to quantify the hydrogen movement velocity in the unloading portion during cyclic loading.

1.2 Why the crack propagation is discontinuous in cyclic loading?

1.3 As the crack propagates, will the hydrogen atoms diffuse out, trap on free surfaces, or just accumulate in the deformed lattice?

1.4 What is the relationship between the crack propagation and hydrogen diffusion? How to quantify them?

1.7 Research objectives

My research will focus on the loading interactions effects on H movement in the NNpHSCC with MD simulations. Considering the others' work in SCC group, several issues required to be resolved are: the under loading effect on fracture mode of crack; minor cycles effects in enhancing crack growth; overloading-retardation effects; H effect on fracture energy and stacking fault energy which related to ductile or brittle failure of steel. More fundamental research will be done to study the hydrogen movement near crack tip and a model which hydrogen atoms accumulate into plastic zone will be verified. Furthermore, the purpose of our research is to explore hydrogen embrittlement mechanisms in NNpHSCC and try to bridge the nano-scale simulations with field operations. Figure 1.14 shows our research objectives, and the most urgent work is colored in red, i.e., quantifying the hydrogen concentration gradient's effects on hydrogen movement and pressure fluctuations generated from cyclic loading on hydrogen movement.

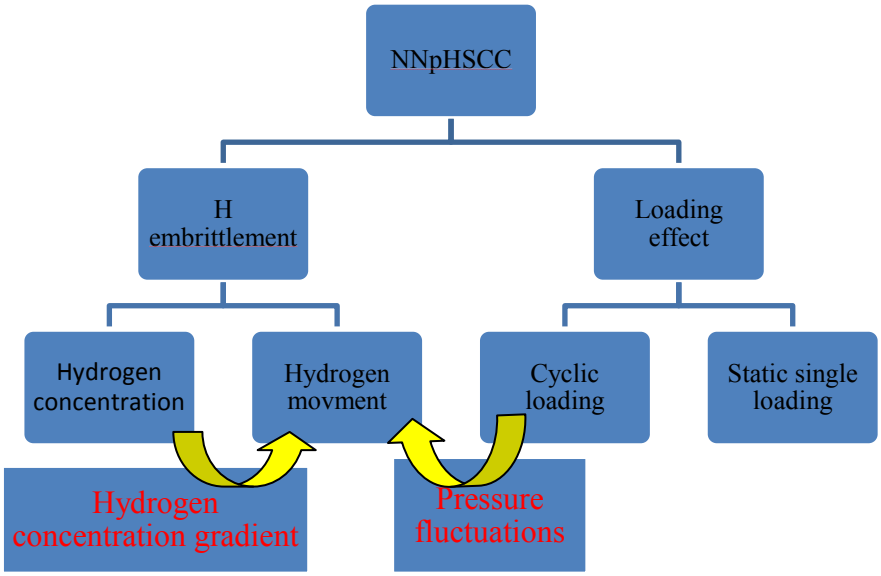

Figure 1.14 Research objectives in the thesis, the most urgent work is colored in red, i.e., quantifying the hydrogen concentration gradient's effects on hydrogen movement and pressure fluctuations generated from cyclic loading on hydrogen movement.

Chapter II Simulation methodology

As introduced above, MD method can acquire insights into atomic level process. With numerical integration of Newton's equations of motion for each atom, the physical properties' change, such as potential energy, stress, structure, can be predicted. The techniques of applying MD simulations in our research will be described in the following paragraphs.

2.1 Newton's equation of motion

Statistic mechanics is the basis for MD simulations. The Hamiltonian H is a sum of kinetic energy in a set of momentum *p* and potential energy in functions of coordinates *q*.

$$H(p,q)=K(p)+\mu(q) \ , \qquad [2.1]$$

$$H=\sum_1^f 0.5m_i\, v_i^2+\mu(q_1....q_f), \qquad [2.2]$$

where *K* is kinetic energy, μ is potential energy and *f* is a degree of freedom, *m* is mass and *q* is coordinate, *p* is momentum. Make differential on both sides for Eq. [2.1] with respect to *t* (*t* is time).

$$\frac{\partial H}{\partial t}=\sum_1^f m_i v_i \frac{\partial v_i}{\partial t}+\sum_1^f \frac{\partial q_i}{\partial t}\frac{\partial \mu}{\partial q_i}, \qquad [2.3]$$

H is time-independent. If only considering one dimension, employing a_i and v_i to replace the differential expression $\frac{\partial v_i}{\partial t}$ and $\frac{\partial q_i}{\partial t}$, the expression could be described as

$$0=m_i v_i a_i+v_i \frac{\partial \mu}{\partial q_i}, \qquad [2.4]$$

or Newton's equation $F=m_i a_i$. Eq. [2.1] has shown the inputs needed to conduct simulations. Especially, the interatomic potential μ would directly determine the reliability of MD simulations.

2.2 Potentials

In molecular physics, the Born–Oppenheimer (BO) approximation is the assumption that the motion of atomic nuclei and electrons in a molecule can be separated. Based on this assumption, there are two types of potentials for general usage. The first one came from solving Schrodinger equation for the electrons; the other one depends on the position of nuclei and usually obtained through fitting experimentally measured data or through more accurate calculation such as first principle. The latter is so called empirical potential which is used in current thesis study. There are mainly two types of empirical potentials in modeling solids: pair potential[54] and many-body potential [55]. Lennard-Jones is a classical pair potential [56][57] shown as

$$\mu = 4\varepsilon\left(\left(\frac{\sigma}{r}\right)^{12} - \left(\frac{\sigma}{r}\right)^{6}\right) \qquad [2.5]$$

where ε is the depth of the energy well and σ is the interparticle spacing when the pairwise potential equals zero. The term $\left(\frac{\sigma}{r}\right)^{12}$ is repulsion part, dominating at short distance when atoms are close; and attraction part $\left(\frac{\sigma}{r}\right)^{6}$ dominates at large distance. Many-body potentials such as embedded atom potential is much more complicated, however will be better in describing metal's properties compared with pair potential. The expression of EAM potential [58–60] is listed as follows

$$U = \frac{1}{2}\sum_{i,j(i\neq j)} \mu_{ij}(r_{ij}) + \sum_{i} G_i(\rho_i); \rho_i = \sum_{i\neq j} \rho_j^a(r_{ij}) \quad [2.6]$$

where $\mu_{ij}(r_{ij})$ is pairwise potential between atom i and j with separation r_{ij}. $G_i(\rho_i)$ represents the energy required for embedding an atom i into uniform electron density ρ_i, while ρ_i is the spherically averaged atomic electron density at atom site i created by all of the rest atoms in the system. The potential used in this thesis is based on the Fe potential which is developed by Mendelev [60], and an extensive database of energies and atomic configurations from the density functional theory (DFT) calculations have been used to fit the cross-interaction of H and Fe [59].

There are some other models for specific usage. For example, the materials in chemical environment may undergo chemical reactions involving the bond breakings and formations, the Reaxff model [61] which is based on the bonding order could be used; The Adaptive Intermolecular Reactive Empirical Bond Order potential (AIREBO) [62] for hydrocarbons has been widely used to study dynamic bonding processes under ambient conditions; the Tersoff potential [63] which is still based on the concept of bond order: the strength of a bond between two atoms is not constant, but depends on the local environment.

2.3 Integration algorithms for molecular dynamics

The potential energy is function of atoms' positions. To integrate the equation of motion, several numerical algorithms have been developed. They are listed as Verlet algorithm [64][65], Velocity-Verlet algorithm [66], Leap-frog algorithm [67], Predictor-corrector algorithm [68]. Since Velocity-Verlet algorithm is one of the commonly used integration

methods and has been used in our study, only original Verlet and Velocity-Verlet algorithms will be introduced here. Verlet algorithms are shown below,

$$r(t+\Delta t)=2r(t)-r(t-\Delta t)+a(t)\Delta t^2+O(\Delta t^4) \quad [2.7]$$

While the equation is only related to positions, the truncation error by Δt is of the fourth order. The velocity obtained from the position is shown as,

$$v(t)=\left(\frac{r(t+\Delta t)-r(t-\Delta t)}{2\Delta t}\right)+O(\Delta t^2) \quad [2.8]$$

The accuracy of the velocity is on the order of $O(\Delta t^2)$. The Velocity-Verlet algorithms are in the form of Eq. [2.9]

$$r(t+\Delta t)=r(t)+v(t)\Delta t+(1/2)a(t)\Delta t^2 \quad [2.9]$$

and Eq. [2.10]

$$v(t+\Delta t)=v(t)+\frac{1}{2}[a(t)+a(t+\Delta t)]\ \Delta t\,, \quad [2.10]$$

This scheme has the same accuracy for predicting positions and predicting velocity. The accuracy of estimation would be up to Δt^4 for both velocities and positions estimation in Velocity-Verlet algorithm, while the accuracy of original Verlet algorithm in velocity prediction is just Δt^2.

2.4 Temperature control

NVT (canonical ensemble) [69] is used in our simulations in which number of molecules, volume of system and temperature are conserved. Variety kinds of means are available for maintaining temperature. The approach employed in our simulation could be expressed as follows.

The Nose-Hoover method is used in this thesis. This is an extension of Nose formulism and is upgraded by Hoover in 1985 [70]. This is an extensive method by introducing an extra degree of freedom that represents the heat bath. The extra degree is dimensionless and is denoted as s. The potential energy and kinetic energy related to s are displayed as $\mu_s = (f+1)k_B T \ln s$ and $K_s = \frac{1}{2}Q\dot{s}$, where Q is the thermal inertia that controls rate of temperature fluctuations. The extended system Hamiltonian is conserved and the extended system is microcanonical which means the internal energy is conserved, too.

Velocity rescaling is a method based on velocity-temperature relationship and is used in equilibrating a system before starting a simulation. The equation is shown below:

$$<\sum_i \frac{1}{2} m v_i^2> = \frac{3}{2} N k_B T \qquad [2.11]$$

where m is the mass; v_i is the velocity of i^{th} atom; N is the number of atoms in system. The velocity of atoms at any instance can be controlled through controlling the temperature. The proportion of the velocity at time T and at time Ti can be expressed as $\sqrt{\frac{T}{T_i}}$.

2.5 Boundary conditions and loading input

In MD simulations, it is either impossible or necessary to simulate the whole materials system. Generally we only choose a region in the system to conduct the simulations, which definitely has certain boundary conditions with surrounding system. Improper sets of boundary conditions may introduce non-physical influences on the simulation system. Commonly there are several different types of boundary conditions, e.g., the fixed boundaries, the periodical boundaries, the flexible boundaries and the free surfaces.

In our simulations, a typical model is first constructed with x, y and z crystallographic directions, respectively. If the initial crack is located in the middle of the z direction and growth along x direction, then this model is built with free surfaces boundary conditions along the x direction, and periodic grain boundary (PBC) [71][72] conditions along the y direction. A constant displacement load is applied to several layers of fixed atoms at two ends of the z direction to correspond to anisotropic elastic mode I stress intensity field K_I.

The system is in plain strain condition and the periodic on y direction is realized by introducing an infinite space-filling array of identical copies of the simulation region. By using PBC, each particle i in the box interacts not only with other particles but also interacts with their images in nearby box. The interactions "go through" box boundaries. In practice, potentials usually have a cutoff distance where short interaction range is defined. It is called minimum image criterion which reduced additional complexity introduced by employing periodic boundary condition.

2.6 Stress calculation

Based on the correlation of hydrostatic stress near the crack tip and hydrogen concentration, the hydrostatic stress should be quantified firstly. In this thesis study, only normal stress is concentrated as the hydrostatic stress [73] formulation is show as $\sigma^{hyd} = \frac{1}{3}\left(\sigma_{xx} + \sigma_{yy} + \sigma_{zz}\right)$.

The loading condition used in the thesis is displacement loading. Only normal stress along loading direction should be substituted into following equations as quantifying the loading stress intensity.

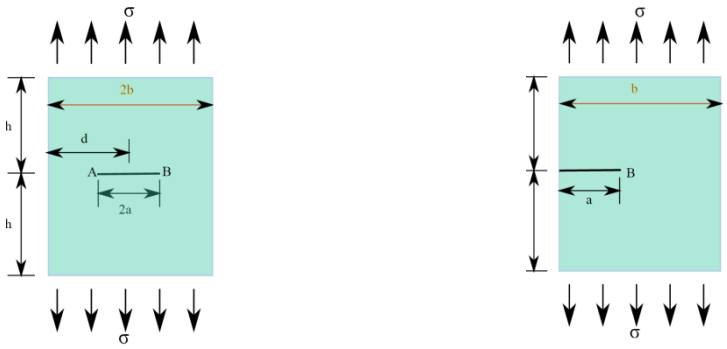

(a) (b)

Figure 2.1 (a) Geometry of a central crack in finite plate, 2a is the length of the crack; (b) geometry of an edge crack in a plate under uniaxial stress. [71]

If a crack located centrally on a finite plate (d=b), the stress intensity could be quantified as following [74],

$$K_I = \sigma\sqrt{\pi a}\left[\frac{1-\frac{a}{2b}+0.326\left(\frac{a}{b}\right)^2}{\sqrt{1-\frac{a}{b}}}\right] \qquad [2.12]$$

The stress intensity expression for a edge crack with crack length *a,* and $a/b<=0.6$, is shown as

$$K_I = \sigma\sqrt{\pi a}\left[1.12-0.23\left(\frac{a}{b}\right)+10.6\left(\frac{a}{b}\right)^2-21.7\left(\frac{a}{b}\right)^3+30.4\left(\frac{a}{b}\right)^4\right] \qquad [2.13]$$

The stress intensity for a edge crack with crack length *a,* and $a/b>0.3$, is expressed as

$$K_I = \sigma\sqrt{\pi a}\left[\frac{1+3\frac{a}{b}}{2\sqrt{\pi\frac{a}{b}}\left(1-\frac{a}{b}\right)^{3/2}}\right] \qquad [2.14]$$

2.7 Mathematical model

The plastic zone shape under plain strain condition can be approximated to be a circular region with radius r_p (as shown in Fig.2.2), which is reasonable because when the H concentration in the circular region reaches equilibrium, its concentration in the plastic zone also reaches saturation. To reach the dynamic equilibrium of hydrogen concentration in the plastic zone during cyclic loading, an annulus region with the inner radius r_p and the outer radius R_{eq} is needed to supply and deplete hydrogen atoms. The hydrogen concentration outside of plastic zone is estimated to be c_0. Therefore, the minimum time, $t_{critical}$, for H diffusion in/out of circular region during cyclic load to satisfy the dynamic equilibrium hydrogen concentration in plastic zone is related to critical frequency through $f_{critical}=1/(2t_{critical})$. Considering equilibrium condition, the hydrogen concentration near crack tip is related to the hydrostatic stress distribution [74,75]. Here we employ the criteria that when the atomic ratio reaches 1, the free surface forms and the crack propagates[22,28].

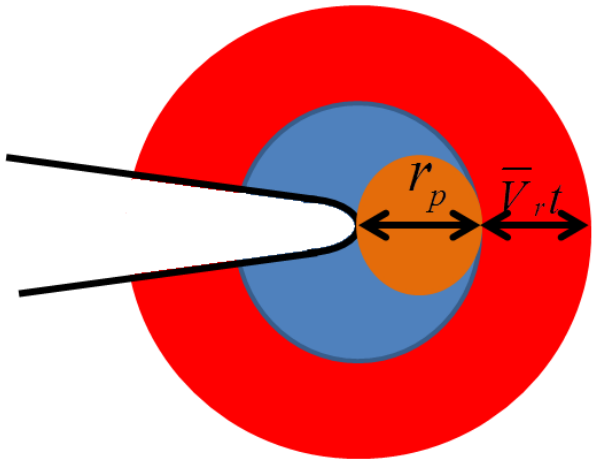

Figure 2.2 The geometry of a crack, where the orange circular region is the plastic zone, and the blue region is a circle region where the radius is equal to r_P. If the blue region is

saturated, the plastic zone will be saturated, too. The red annulus region is to offer and deplete the hydrogen atoms. If hydrogen concentration in the red region reached $c_{critical}$ and the loading time t reached $t_{critical}$, the plastic zone would be saturated in a mode I loading.

The diffusivity of hydrogen atoms outside the plastic zone is assumed to be constant since these regions are not stress concentrated. As the stress intensity changes from K_{min} to K_{max} in a range of time t, the hydrogen atoms can diffuse into the plastic zone from a farthest position r_P+R_{eq}. The total volume of the annulus red region in Fig. 2.2 which offers hydrogen atoms to the plastic zone during loading can be estimated as $l_z[\pi(r_p+R_{eq})^2-\pi r_p^2]$, where $R_{eq}=\bar{V}_r*t$ and $\bar{V}_r$ is the hydrogen moving rate. There are not a lot plastic deformations outside the plastic zone, hence the red region is assumed to be in bcc structure. And the total number of Fe atoms contained in the red region is $l_z[\pi(r_p+R_{eq})^2-\pi r_p^2]/(a_o^3/2)$, where $a_o^3/2$ is the volume taken by each Fe atom. Total hydrogen atoms to saturate the plastic zone is euqal to atomic ratio of H/Fe (c_o) multiplying the number of Fe atoms.

Chapter III Atomistic simulation of hydrogen-assisted ductile-to-brittle transition in α-iron

3.1 Introduction

Hydrogen embrittlement (HE) [21,26,76] in iron (or steel) is a phenomenon in which the material loses ductility and becomes brittle, and is one of the most severe steel degradation mechanisms. Experimental results and theoretical studies have led to an understanding of ductile-to-brittle transition from both hydrogen-enhanced local plasticity (HELP) [20,22,23,44,77] and hydrogen-enhanced decohesion (HEDE) [11,13,23,28,51,78], where hydrogen atoms not only enhance the motion of dislocations which increases local stresses, but also diminish the bonding energy between adjacent iron atoms that causes planar failure. Because of the high mobility of H in Fe [49,79,80], it is natural to postulate that DTB transition is related to hydrogen diffusivity and accumulation [29,81]. In addition, molecular dynamics (MD) simulations suggest that HE is related to the accumulation of H atoms in tensile stress fields. This accumulation effect not only enhances the pinning effect to dislocations, which harden the material [76], but also decreases the free surface energy and stacking fault energy simultaneously near the crack tip [10]. The mechanism can be expressed using two parameters, K_I^e and K_I^c, the stress intensity factors associated with the first emitted dislocation from the crack and with crack cleavage, respectively. For a given material, if K_I^e is less than K_I^c, it will deform plastically near a crack tip. However, if K_I^c is less than K_I^e, it will form cleavage near a crack tip. It is also important to note that a change in hydrogen concentration would likely change the free surface energy and stacking fault energy, which would affect the relative values of K_I^c and K_I^e. As a result, it is possible for a ductile material to have a K_I^c smaller than its K_I^e, which results in a ductile-to-brittle transition [28][29].

A version of this chapter has been submitted to *Computational Materials Science* and is under review.

In the current paper, the critical hydrogen concentration required in a steel specimen to have DTB transition occur in a mode I fracture is quantified using MD simulations. It is found that the calculated hydrogen concentration is much larger than that measured in a near-neutral pH stress corrosion cracking (NNpHSCC) environment. Apparently, DTB transition is not observed in mode I fracture single-loading experiments. However, evidence of DTB transition has been observed in cyclic loading in NNpHSCC. Therefore, it is reasonable to expect that a driving force in cyclic loading to accumulate hydrogen atoms in the cracking plane exists and allows DTB transition to occur. This driving force of hydrogen motion must be related to hydrogen concentration gradients and hydrostatic stress distribution [32]. Based on these findings, we expect that HE does not only depend on hydrogen concentration but also on the loading spectrum [82–84].

Since quantitative prediction based on hydrogen accumulation has not been clearly proved, the current work proposes a mechanism of hydrogen saturation in the plastic zone. MD simulations are employed to perform a mode I fracture in bcc iron over a wide range of hydrogen concentrations. Based on these simulation results, a theoretical hydrogen concentration on the crack plane for ductile-to-brittle transition can be estimated using Griffith's theory[74]. This estimated hydrogen concentration can be further used to calculate a theoretical hydrogen concentration in specimens. Based on a hydrogen diffusion model we previously developed to predict the crack propagation rate [85], the theoretical hydrogen concentration can be used to estimate the minimum number of loading cycles that accumulate the hydrogen atoms to make a crack’s ductile-to-brittle transition occurs. A good

agreement between the estimated value and the experimental observation verifies that cyclic loading has an effect on the accumulation of hydrogen atoms and the facilitation of crack propagation.

3.2 Simulation methodology

Two single-crystal bcc iron models are first constructed with crystallographic directions $[\bar{1}10]$ $[\bar{1}\bar{1}2]$ $[111]$ and $[001][110]$ $[\bar{1}10]$ in the x, y and z directions, respectively. Simulation cells comprised of 420000/570000 Fe atoms are 40×2.1×60nm / 40×2.8×60nm in three dimensions. The initial crack is located in the middle of the z direction with [crack front](crack plane normal) directions of $[\bar{1}10]$ (111) and $[001]$ $(\bar{1}10)$. The initial crack length is approximately 100Å and the width of the open mouth is 20Å. A typical model is shown in Fig. 3. 1 (a) with free surfaces boundary conditions along the x direction, and periodic grain boundary conditions along the y direction. A constant displacement load is applied to several layers of fixed atoms at two ends of the z direction to correspond to anisotropic elastic mode I stress intensity field K_I.

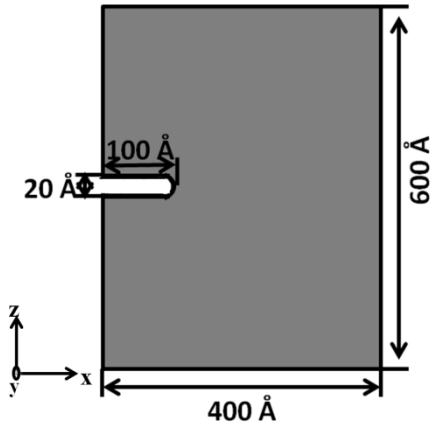

(a)

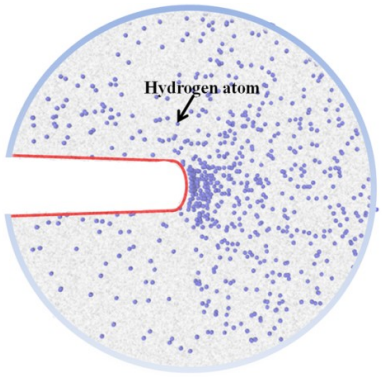

(b)

Figure 3.1 (a) The geometry of the crack in single crystal bcc iron, (b) The hydrogen distribution near crack tip that is determined by hydrostatic stress or stress intensity. The red lines are free surfaces.

MD simulations are performed using a canonical ensemble (NVT)[86], where constant temperature is maintained through the Nose-Hoover method [87,88]. Atomic interactions are described using the embedded atom method (EAM) [89]. The potential is based on the Fe potential from Mendelev [60], and an extensive database of energies and atomic configurations from the density functional theory (DFT) calculations have been used to fit the cross-interaction of H and Fe [59]. All simulations are carried out using LAMMPS code [90]. Based on the literature, the hydrogen atoms are stably located at the tetrahedral sites in bcc iron [91], and the distribution of hydrogen atoms depends on hydrostatic stress, which is shown in Fig. 3.1(b). Hence, hydrogen atoms are introduced into the tetrahedral sites to comply to the hydrostatic stress distribution as following equations show [40]:

$$c_{eq} = \begin{cases} c_o \exp\left(\dfrac{4(1+\nu)K_I\Omega_H}{3\pi k_B T\sqrt{2\pi r}}\right), r \le r_o \\ c_o \exp\left(\dfrac{4(1+\nu)K_I\Omega_H}{3\pi k_B T\sqrt{2\pi r_o}}\right), r > r_o \end{cases} \quad [3.1]$$

where c_{eq} is the equilibrium hydrogen concentration, c_o is the hydrogen concentration away from the crack tip without hydrostatic stress, ν is Poisson's ratio, K_I is the stress intensity, Ω_H is the partial volume of hydrogen in α-iron, k_B is the Boltzmann constant, T is the temperature, r is the distance from a specific position to the crack tip, and r_o is a critical distance value beyond which the hydrogen concentration remains constant in the model. In the current study, we chose c_o from 1×10^{-5} to 0.1 atomic ratio to investigate the appropriate

hydrogen concentration that leads to hydrogen accumulation in our model, where c_o falls into the typical hydrogen concentration range that has been used in previous studies [18][33]. Our simulation results suggest that hydrogen concentration fluctuations over a distance from 0-15nm are much larger than those from 15-30nm. Therefore, we chose 15nm as the r_o for our current simulations. The system is initially deformed to a load 0.8MPa*$m^{0.5}$, which offers the driving force for hydrogen accumulation. As the hydrogen atoms are introduced into the system by hydrostatic stress, the systems are relaxed for 4ns at T = 300K.

3.3 Results and discussion

3.3.1 Plastic deformation and cleavage in α-iron

In Mode I fractures of ductile materials, dislocations will emit before cracks propagate as stress intensity increases. In bcc iron, partial dislocation nucleation will generate stacking faults, which will lead to the formation of full dislocations or twinning partials. Based on the Rice model [29,30], K_I^e depends on the unstable stacking fault energy Υ_{us}. On the other hand, Griffith's theory predicted that K_I^c is related to the free surface energy Υ_s [31]. Therefore, we firstly examine how hydrogen concentration affects the Υ_{us} and Υ_s values.

To calculate the free surface energy, a perfect α-iron single crystal is chosen to contain a concentration (c) of H atoms occupying tetrahedral sites between two planes along which the fracture will occur. The system is then separated into two parts along the plane, where each free surface contains an equal number of hydrogen atoms. The ratio of the energy difference between the intact and separated states to the free surface area yields the free surface energy Υ_s [32]. Since cleavage stress intensity is related to the free surface energy, which is a function of hydrogen concentration and the shear modulus, $K_I^c = \sqrt{\gamma_s / A_I\left(c_{11}, c_{12}, c_{44}\right)}$ [10],

the reduction in the free surface energy results in a reduction in cleavage stress intensity. In Fig. 3.2, simulation results show that the free surface energy of a more closed packed plane {110} is much smaller than that of {111}. As the hydrogen atoms are introduced between two planes, the free surface energy reduces in both planes and the change along the {110} plane is more significant than that of the {111} plane.

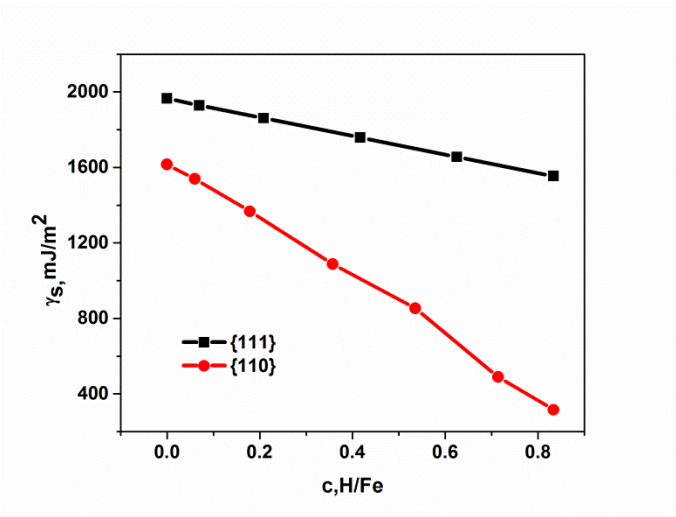

Figure 3.2 Free surface energy γ_s as a function of H concentration for {111} and {110} crack planes.

The two slip systems (i.e., [slip direction](slip plane)) in the current models are $[\bar{1}11](110)$ and $[111](\bar{1}\,\bar{1}2)$, and the corresponding stacking fault energies are calculated as shown in Fig. 3.3. To calculate the stacking fault energy, a perfect α-iron single crystal is chosen to contain a concentration (c) of H atoms occupying tetrahedral sites between two planes along which the slip will occur. The ratio of the energy difference between the intact and slipping states to the free surface area yields the stacking fault energy [95]. The lattice energy changes as a function of slip distance are listed in Figure 3.3(a) and (b) for two orientations.

Figure 3(c) is the stacking fault energy and shows that the hydrogen atoms tend to enhance the dislocation movement in the $[\bar{1}11](110)$ slip system, while hindering motion in the $[111](\bar{1}\,\bar{1}2)$ slip system. These results suggest that it is possible to observe both the HELP phenomenon and hydrogen constraining slipping bands phenomenon [96] in laboratory tests, and hydrogen effects on dislocation emission are somehow orientation-dependent.

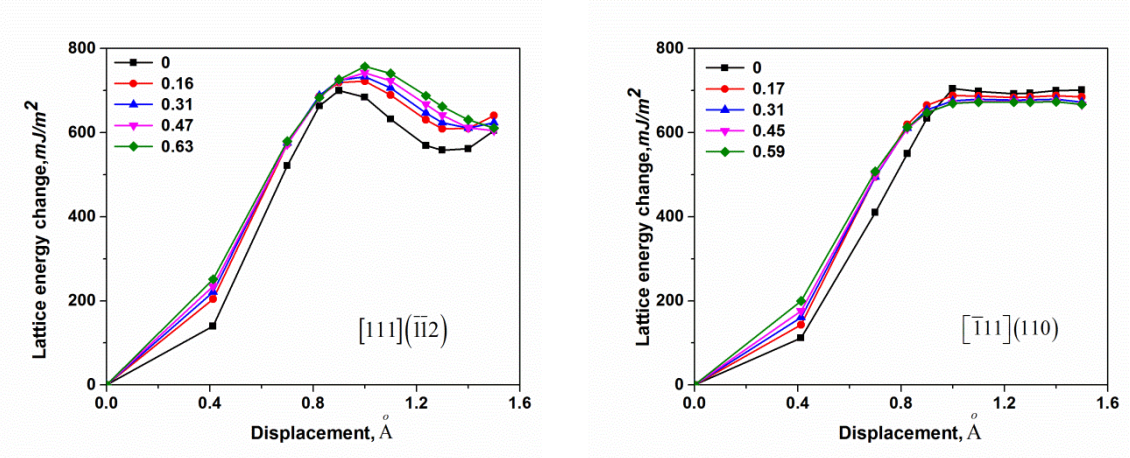

(a) (b)

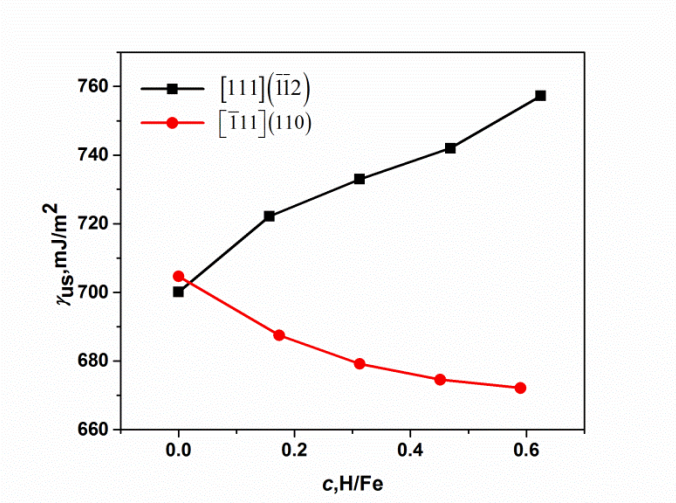

(C)Figure 3.3 (a) Lattice energy versus slip displacement on $[111](\bar{1}\,\bar{1}2)$ slip system; (b) Lattice energy versus slip displacement on $[\bar{1}11](110)$ slip system; (c) The unstable stacking fault energy as a function of atomic hydrogen concentration

3.3.2 Hydrogen effect on cleavage and dislocation emission

We next examine the crack cleavage for two geometries with orientations of $\left[\bar{1}10\right](111)$ and $[001]\left(\bar{1}10\right)$. Each orientation corresponds to a specific dislocation slip system, $\left[\bar{1}11\right](110)$ or $[111]\left(\bar{1}\,\bar{1}2\right)$, respectively. The systems are initially deformed to a stress intensity of 0.8MPa*$m^{0.5}$, which creates a hydrostatic stress field around the crack tip and provides the driving force for hydrogen accumulation. As hydrogen atoms are introduced into the system by hydrostatic stress, we performed a 4-ns relaxation to ensure the hydrogen reaches equilibrium. Then, the crack response to further loading is tested, as both orientations of cracks exhibit a transition from ductile to "brittle" as the hydrogen concentration reaches a critical value. Here, brittle is defined as crack initiation before dislocation emission. The theoretical stress intensities can be calculated using the following equations [92,94]:

$$K_I^e = \frac{1}{\cos^2(\theta/2)\sin(\theta/2)}\sqrt{\frac{2G}{1-\nu}\gamma_{us}\left[1+(1-\nu)\tan^2\phi\right]} \qquad [3.2]$$

and

$$K_I^c = \sqrt{\gamma_s\left[\frac{\sqrt{c_{22}}}{2}\sqrt{2c_{11}+2c_{12}+c_{44}}\right]} \qquad [3.3]$$

where G is the shear modulus that equals to $(c_{11}-c_{12}+c_{44})/3$, Θ is the angle between the dislocation emission direction and crack front direction, ϕ is the angle between the Burgers vector and the vector perpendicular to the crack front direction, and c_{ij} is the elastic modulus. As both equations have shown, K_I^e is positively related to $\sqrt{\gamma_{us}}$ and K_I^c is positively related to $\sqrt{\gamma_s}$ in specific orientations. For both orientations, K_I^e is always smaller than K_I^c when no hydrogen is present, suggesting a ductile deformation. In orientation I, both free surface energy and stacking fault energy decrease as hydrogen concentration increases. Since the

free surface energy changes faster than stacking fault energy, it is expected that K_I^c becomes smaller than K_I^e when hydrogen concentration is higher than a critical value. In orientation II, the free surface energy and stacking fault energy have an opposite trend with hydrogen concentration, suggesting that K_I^c will be smaller than K_I^e beyond a critical H concentration. Therefore, for both cases, it is expected that a ductile-to-brittle transition (K_I^c is smaller than K_I^e) will occur if the hydrogen concentration is high enough.

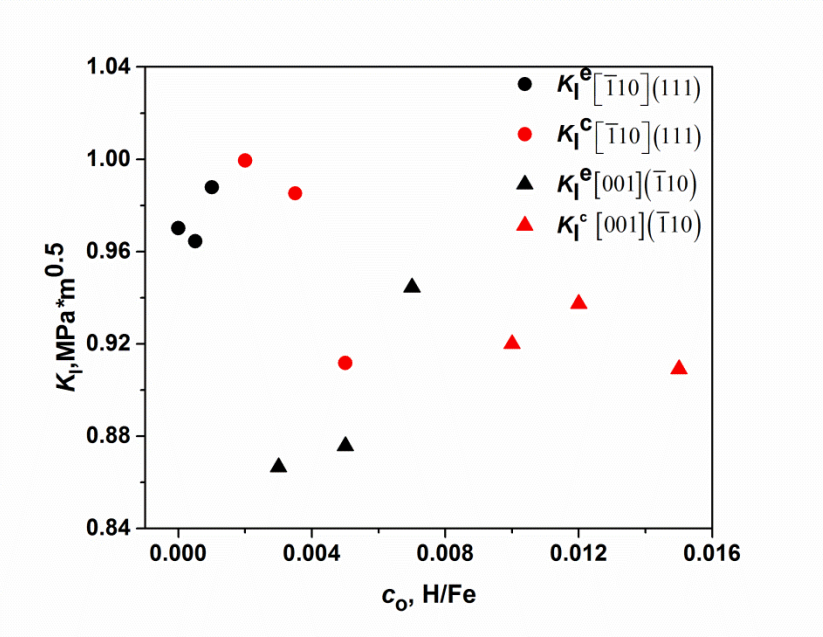

Figure 3.4 The stress intensity versus hydrogen concentration where c_o is the overall hydrogen concentration in the system. The black circles are the K_I^e (dislocation emission firstly) and red circles are K_I^c (crack propagate firstly) values of first orientation, the black triangles are the K_I^e values and red triangles are the K_I^c values of 2nd orientation.

Simulation results show ductile-to-brittle transition in both orientations, as shown in Figure 3.4. It can confirm K_I fluctuates based on Eqs. [3.2] and [3.3]. In Figure 3.5, a hydrogen-rich region forms ahead of the crack tip in nano-level size when c_o increases. However, in Fig.

3.5 (a) where c_o is equal to 0.0035, the cracks are arrested and become blunt again as cracks propagate beyond the hydrogen-rich region. Apparently, a further increase in hydrogen concentration ensures hydrogen-assisted cracking growth, as demonstrated in Fig. 3.5 (a) where c_o is equal to 0.005. However, the crack is classified as "brittle" if it initiates before dislocation emission.

In orientation II, when the hydrogen concentration is very low, the hydrogen atoms diffuse to the free surfaces, which make initiation of a crack very difficult. As the hydrogen concentration increases, the hydrogen-rich region starts to cover the slip systems in the crack front. Then, the crack initiates from the two edges and begins to propagate, as shown in Fig. 3.5(b).

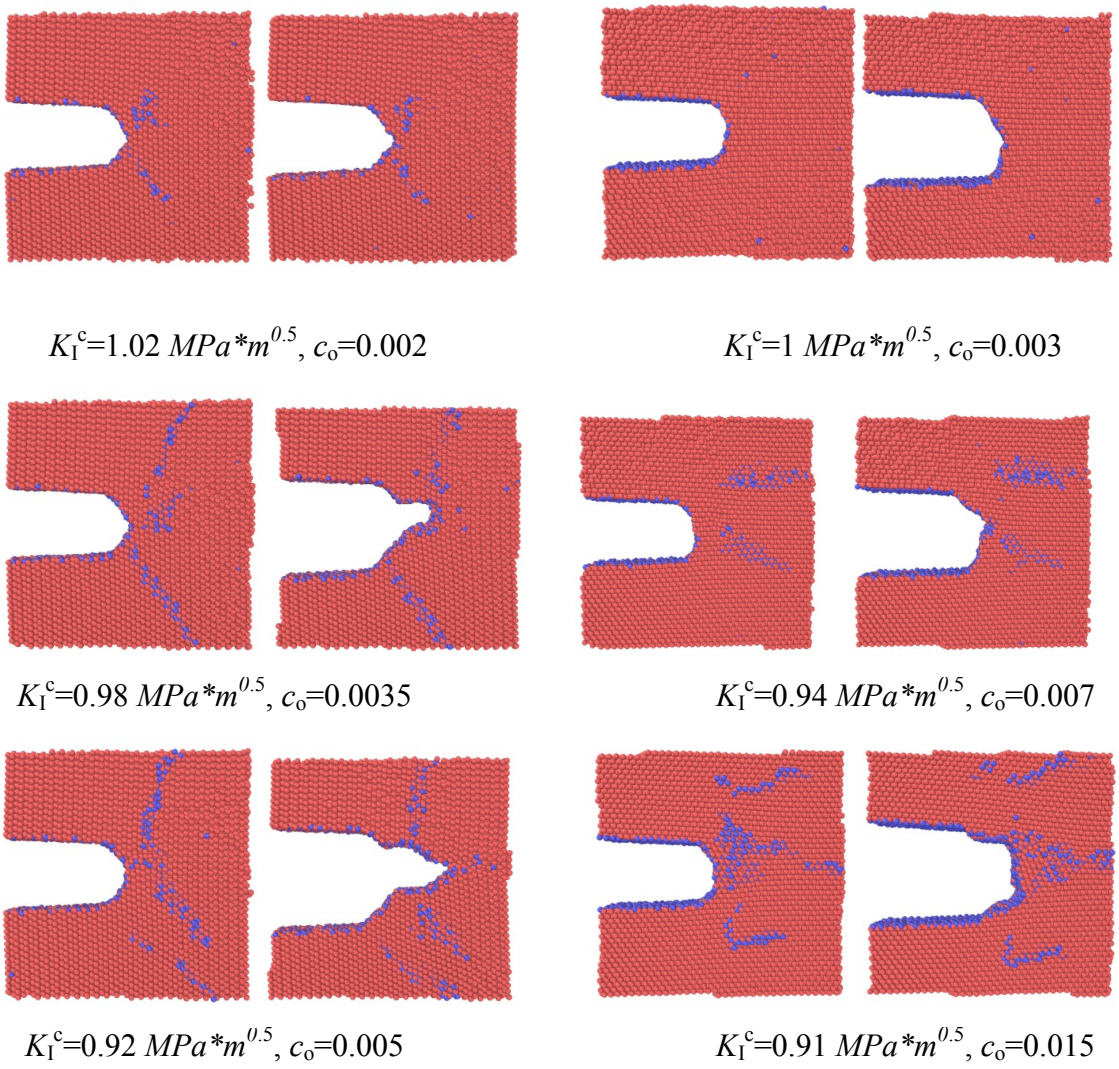

Figure 3.5 (a) Atomistic configurations of crack geometry $\left[\bar{1}10\right]\left(111\right)$. The side length of the curvature R is 5 nm, the blue atoms represent hydrogen atoms and the red atoms are iron. (b) Atomistic configurations of crack geometry $\left[001\right]\left(\bar{1}10\right)$. The radius of the curvature R is 5 nm.

To further confirm that DTB transition in MD simulations requires the local hydrogen concentration to reach a critical value, we examined the hydrogen atomic concentration in a

nano-sized region ahead of the crack tip in a function of simulation time. The simulation results in Fig. 3.4 suggest that in orientation I, DTB transition occurs when the overall H concentration (c_o) is greater than 0.002. In Fig. 6 (a), we observe that the local atomic hydrogen concentration reaches 0.3-0.4 before the cracks become cleavage in all cases. For orientation II, Fig. 3.4 suggests the critical overall concentration is approximately c_o=0.007. In Fig. 3.6 (b), when c_o=0.007, the crack becomes "brittle" as the hydrogen concentration approaches 0.4 at the crack front direction. When c_o=0.015, the hydrogen concentration ahead of the crack tip is 0.5 and the crack is always brittle. When c_o=0.003, the local H concentration cannot reach the critical value, so it stays ductile.

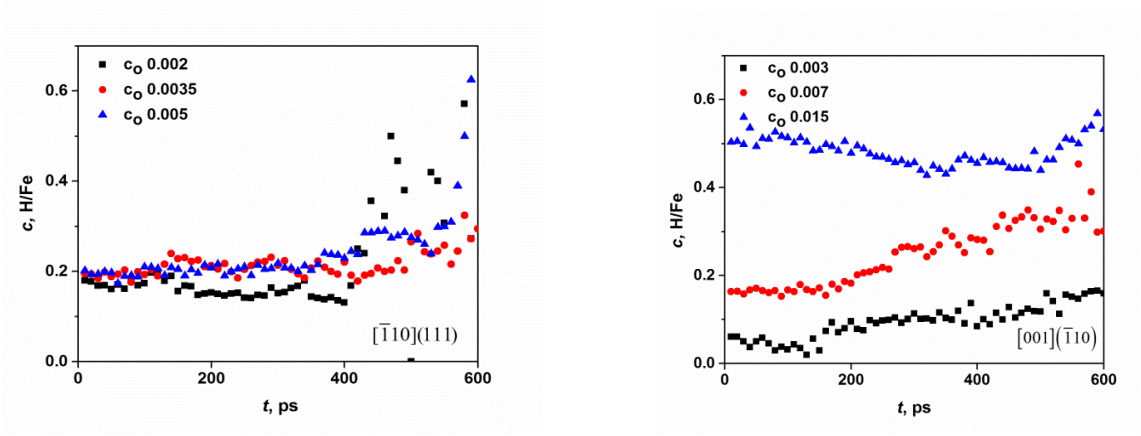

(a) (b)

Figure 3.6 Fluctuations of hydrogen atomic concentration in a nano-size region ahead of crack tip versus time. The hydrogen fluctuations show the DTB transition tendency and mark the threshold of hydrogen concentration.

The local critical H concentration that leads to DTB transition can also be estimated using Griffith's theory. Griffith's theory applies the energy balance idea to the formation of a crack as a plate subjected to a constant stress, i.e., the increased potential energy Π should be converted to the energy required to open the crack [25]. The total energy is conserved, while

the applied elastic energy becomes the free surface energy as the material is brittle. That being said, Griffith's theory could, therefore, be applied to predict K_I^c values as the H-charged crack becomes brittle by using Eq. [3.4]:

$$K_I^c = \sqrt{2E\gamma_s} \qquad [3.4]$$

where E is Young's modulus (varies with orientation). For instance, we apply Griffith's theory to the geometry in orientation I, as shown in Fig. 3.6 (a). The K_I^c value corresponding to the initiation of a nano-sized crack is 0.92MPa*$m^{0.5}$ and E is equal to 250GPa in this orientation. Using Eq. [3.4], when the transition occurs, the free surface energy γ_s corresponds to c ~ 0.4, as shown in Fig. 3.2. It is consistent with all the observations presented above. For further calculations, we choose c=0.4 as the critical value for DTB transition in iron.

3.3.3 Critical hydrogen concentration in the specimen and total number of hydrogen atoms required to saturate the plastic zone

The local hydrogen concentration on the crack surface beyond which the crack will propagate by cleavage is an atomic ratio of approximately 0.4. It has been calculated from MD simulations. If the value of r, or the size of the hydrogen-rich region, is taken as 1nm in Eq. [3.1], the c_o value, which is the critical hydrogen value in a specimen required to cause DTB transition in Mode I loading, is estimated as 244 ppm. Furthermore, the number of hydrogen atoms required to saturate the plastic zone can be estimated using Eq. [3.5] [14, 33].

$$N_h = \int_{K_{\min}}^{K_{\max}} \int_0^{r_p} \frac{c_{critical} \exp\left(\frac{\sigma^{hyd}\Omega_H}{k_B T}\right) 2\pi r l_z}{a_0^3/2} dr,$$

$$\sigma^{hyd}(r,\theta)=\frac{1}{3}\left(\sigma_{xx}+\sigma_{yy}+\sigma_{zz}\right)=\frac{2(1+v)}{3\sqrt{2\pi r}}K_I cos\frac{\theta}{2} \qquad [3.5]$$

where N_h is the number of hydrogen atoms required to saturate the hydrostatic stress concentrated zone, r_p is the size of the plastic zone, l_z is the thickness of specimen, a_o is the lattice parameter and r is the radius to crack tip. Note that the value N_h is underestimated because of the pinning effects of dislocation cores [76], and the free volume in GBs also aids in the trapping of hydrogen atoms. If we consider the hydrogen atoms trapped in dislocation cores as the dislocation density, which is taken to be approximately $10^{-15}/m^2$ [98], then extra hydrogen atoms required to saturate the plastic zone can be calculated as follows [7]:

$$N_d=10^{15}*\pi*r_p^2\int_0^{d/2}\frac{c_{critical}\exp\left(\frac{p\Omega_H}{k_BT}\right)2\pi r l_z}{a_0^3/2}dr,\ P(r,\theta)=-\frac{(1+v)Gb}{3\pi(1-v)}\frac{\sin\theta}{r} \qquad [3.6]$$

where N_d is the number of hydrogen atoms trapped by dislocation cores, P is the stress field of dislocation, d is the size of the dislocation core, which is approximately 9Å, b is equal to $\sqrt{3}a_o/2$ and r is the distance from a specific position to the dislocation core. Calculations suggest that 15% more hydrogen atoms are required to saturate these dislocation cores, compared with those required to saturate the concentrated hydrostatic zone. Therefore, the corrected critical hydrogen concentration in the whole system that causes DTB transition is ~280ppm. Using this value to represent the $c_{critical}$ in Eq. [3.5] and [3.6], the total number of hydrogen atoms that are required to saturate the plastic zone can be calculated. Note that this value is still underestimated because the minor cycles will generate plastic deformations and defects in the plastic zone, which can trap hydrogen atoms with the increments of minor cycles [99][100] .

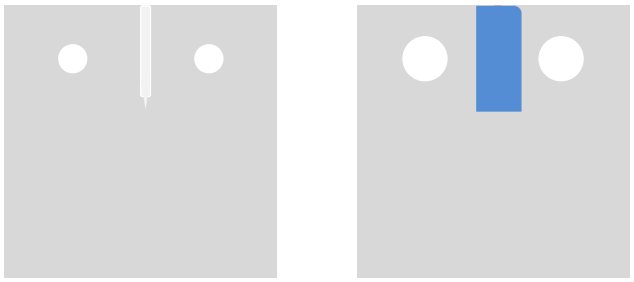

(a) (b)

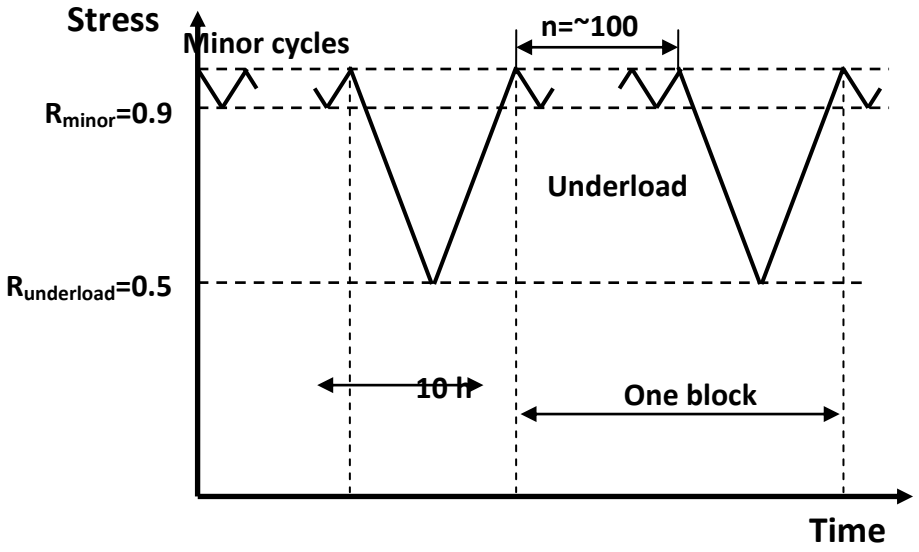

(c)

Figure 3.7 Experimental (a) surface treated compact tension specimen; (b) compact tension specimen with covered crack which ensure no corrosion happens during loading; and (c) variable amplitude waveform: Kmax=33 MPa√m, R ratio of minor cycles=0.9, R ratio of underload=0.5, frequency of minor cycles=0.00538 Hz, frequency of underload=0.0000278 Hz (10h/cycle), number of minor cycles per block n=1000. [24]

Based on experimental observations, hydrogen concentrations in a near neutral pH (NNpH) environment can only reach up to 2ppm outside of the plastic zone [26]. It seems impossible

to have a ductile-to-brittle transition in NNpH environment due to the overall low hydrogen concentration. However, evidence of ductile-to-brittle transition has been observed in recent cyclic loading laboratory tests using X65 steel compact tension (CT) specimens with a thickness of 9±0.2mm. The CT specimens are ground to a 600-grit finish and then pre-cracked by fatigue in air to produce a crack tip that shows a similar microstructure in MD simulations. The notch and crack region of the specimen are shown in Fig. 3.7(a) [38]. These specimens are exposed to a near-neutral pH solution (C2 solution) during tests, which ensures the hydrogen concentration in the specimen is 2ppm [39]. Corrosion would likely destroy the crack plane structure (striations) as the loading time is long (*n* is large). Parallel tests using a covered crack, shown in Fig. 3.7 (b), were also carried out to inspect the crack plane structure at *n*=1000. A bare specimen is also tested in air for the purpose of comparison.

An underload-minor cycle-type variable amplitude cyclic loading waveform, as shown in Fig. 3.7 (c), is designed to simulate actual pressure fluctuations during pipeline routine operations. The starting mechanical loading conditions are as follows: the maximum stress intensity factor, K_{max}=33MPa√m, R ratio (minimum stress/maximum stress) of minor cycles=0.9, R ratio of underload=0.5, frequency of minor cycles=0.00538Hz, frequency of underload=0.0000278Hz (10h/cycle), and number of minor cycles per block *n* ranged up to 1000. Minor cycles with a large R ratio will generate few free surfaces, and these cycles simulate not only the actual loading condition, but also the hydrogen-saturation condition in MD simulations.

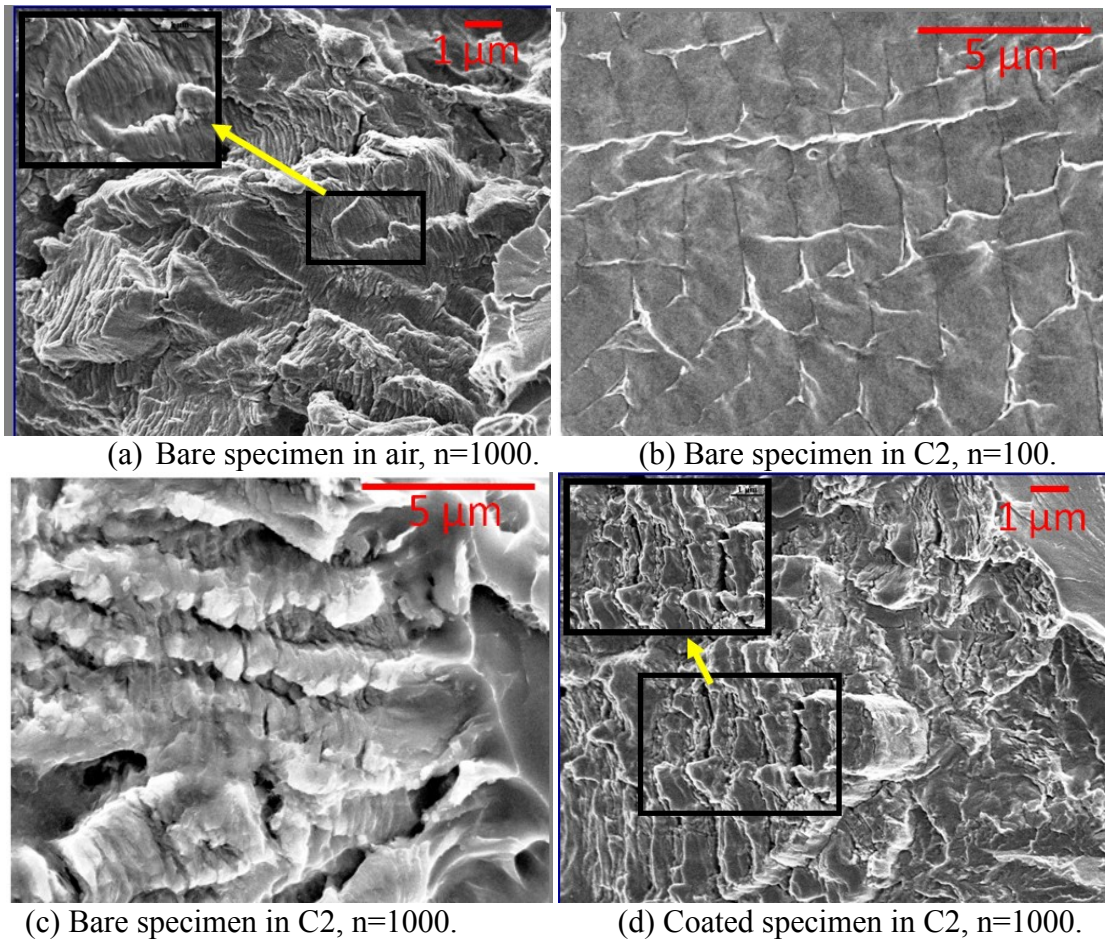

(a) Bare specimen in air, n=1000. (b) Bare specimen in C2, n=100.

(c) Bare specimen in C2, n=1000. (d) Coated specimen in C2, n=1000.

Figure 3.8 Fracture surfaces images near the crack tip after tests (crack propagation from left to right). The inset is a magnified view of the fracture surface. Large spaced striations can be detected in the coated specimen and in the bare specimen (n is small) in C2 solution. [24]

Fractured surfaces in the middle section of specimens are examined and shown in Fig. 3.8. Mini-striations are observed over the entire surface for the bare specimen tested in air as n=1000, which confirms that crack advancement is caused by the mechanism of fatigue alone. On the other hand, the fractured surface of the specimen tested in C2 exhibits a combination of quasi-cleavage, where large-spaced striations and mini striations are alternatively arranged. When the number of minor cycles n is small in C2 solution, there are

only large-spaced striations (beginning of DTB transition), as shown in Fig. 3.8 (b) (bare sample). There is a critical value of *n* (around 700), shown in Table 1 and Fig. 3.9, beyond which the crack growth rate per block will be maximized. This critical value marks the saturation of the plastic zone with hydrogen atoms after the accumulation of 700 minor cycles and the appearance of a DTB transition. If *n* further increases, not so much change will occur in the length of the large-spaced striations, as shown in Fig. 3.8 (d), nor will the crack growth rate.

In Mode I loading, ductile-to-brittle transition is impossible because the overall hydrogen concentration is very low in NNpH environment compared with the local critical hydrogen concentration. However, it is possible that hydrogen atoms are able to accumulate in the plastic zone during cyclic loading and form a hydrogen-rich region. The cracks stay dormant during minor cycles which offer a stable zone for hydrogen accumulation. At the beginning of loading, the hydrogen concentration at the crack tip is low and the hydrogen concentration gradient can be neglected. Hence, the movement velocity of hydrogen atoms is only related to stress distribution, as Eq. [3.7] describes:

$$V_r^{\sigma} = \frac{DF_r}{k_B T} = \frac{(1+v)\Omega}{k_B T 3\sqrt{2\pi}} \frac{DK_I \cos\frac{\theta}{2}}{r^{3/2}}, \quad F_r = -\nabla\mu = -\Omega\nabla\sigma^{hyd} \qquad [3.7]$$

where μ is the chemical potential of hydrogen atoms in iron, and r is the size of the plastic zone. With the increments of minor cycles, the hydrogen atoms accumulate near the crack tip, however, the hydrogen concentration is much smaller than the equilibrium value as number of minor cycles (n) is small. The tensile stress field still accumulates hydrogen atoms. However, as n reaches a critical value where the plastic zone is saturated, the

hydrogen atoms may diffuse out and the moving rate is related to both the hydrogen concentration gradient and the stress field. The hydrogen-moving rate related to concentration gradient as hydrogen concentration reaches equilibrium is shown in Eq. [3.8]. During the unloading, the positive stress intensity will still provide driving force for accumulating hydrogen atoms because hydrogen concentration has not reached equilibrium.

$$V_r^c = -D\nabla \ln\left(\frac{c_{eq}}{1-c_{eq}}\right) = \frac{-D}{c_{eq}(1-c_{eq})}\nabla c_{eq} = \frac{1}{1-c_{eq}} V_r^{\sigma} \qquad [3.8]$$

However, c_{eq} is much smaller than 1 near the boundary of plastic zone, hence, the V_r^c has similar amplitude with the Vr^{σ} but in opposite directions (The derivations of both velocities have been included in the Appendix). Hydrogen atoms are very difficult to diffuse out even reaching equilibrium. Therefore, the number of hydrogen atoms in the plastic zone increases in each minor cycle until a brittle cleavage occurs. As the crack grows through the hydrogen-rich region after brittle cleavage, it becomes ductile and dormant again, a new hydrogen accumulation process restarts. The seperated large-spaced striations (quasi-cleavage) on the cracking planes in Fig. [3.8] verify this discontinuous crack-propagation mechanism.

3.3.4 Calculation of the number of minor cyles to achieve a ductile-to-brittle transition

A comparison of the crack plane in air and in C2 solution, which is shown in figure 3.8, suggests that the cracks change from ductile to brittle as the number of minor cycles increases. Furthermore, a critical value of minor cycles under a specific stress intensity and hydrogen concentration was found in experimental tests, and ductile-to-brittle fracture surfaces (large-spaced striations seperated with minor cycles) can be observed in tests if the number of cycles exceeds this critical value. As shown in Section A, the overall hydrogen concentration required to make DTB transition occur in Mode I loading can be estimated using MD simulations. Applying this estimated hydrogen concentration value to laboratory

tests' loading conditions, the number of hydrogen atoms required to saturate the plastic zone and make the transition occur can be calculated with Eq. [3.5] and [3.6].

The actual value of hydrogen atoms diffusing into the plastic zone in one minor cycle (R=0.9) is approximately equal to the number of hydrogen atoms diffusing into the plastic zone during loading, as the hydrogen escaping rate is very small in comparison to the hydrogen accumulation rate as described in section C. Then, the number of hydrogen atoms diffusing into the plastic zone in one minor cycle can be expressed as

$$N_H^{\min or cycle} = \frac{c_o l_z \left[\pi \left(r_p + \overline{V}_r * t \right)^2 - \pi r_p^2 \right]}{a_o^3 / 2} \quad , \quad \overline{V}_r = \frac{\int_{K_{\min}}^{K_{\max}} V_r(K_I, r_p) dK_I}{K_{\max} - K_{\min}} \qquad [3.9]$$

where $\overline{V}_r$ is the average hydrogen-movement velocity at the boundary of the plastic zone. As R=0.9, f_{critical} is 0.0032Hz and t_{critical} of the minor cycle is 154s, which is longer than the laboratory test loading time of ~ 93s. The details of the assumptions in calculating the hydrogen diffusion in plastic zone in each minor cycle and an alternative method to calculate the hydrogen atoms required to saturate plastic zone have been described in the Appendix. In laboratory tests, if the loading time is less than t_{critical}, the number of accumulating hydrogen atoms can be related to time t. Hence, the loading time t used in Eq. [3.9] is 93s and c_o is 2ppm [101] in the specimen. To make an accurate prediction, we also need to consider the number of hydrogen atoms that diffused to the formed free surfaces. In laboratory tests, the propagation distance, Δa, for large-spaced striations is approximately $1*10^{-6}$m. The atomic ratio (H/Fe) of hydrogen concentration on the free surface is approximately 1 [22], and the number of hydrogen atoms diffusing to the free surface is as follows:

$$N_H^{freesurface} = \frac{2\Delta a l_z}{\pi\left(3a_o^3/8\pi\right)^{2/3}} \quad [3.10]$$

which appears to be very low compared with N_H^{total} (N_h+N_d) and can be neglected in calculations. This suggests that as the crack grows beyond the hydrogen-rich region, more hydrogen atoms can diffuse out or stay in the lattice compared to those on the free surfaces. Hence, the predicted value of minor cycles required to make the ductile-to-brittle transition occur is equal to $\frac{N_H^{total}}{N_H^{minorcycle}}$, or 657 cycles.

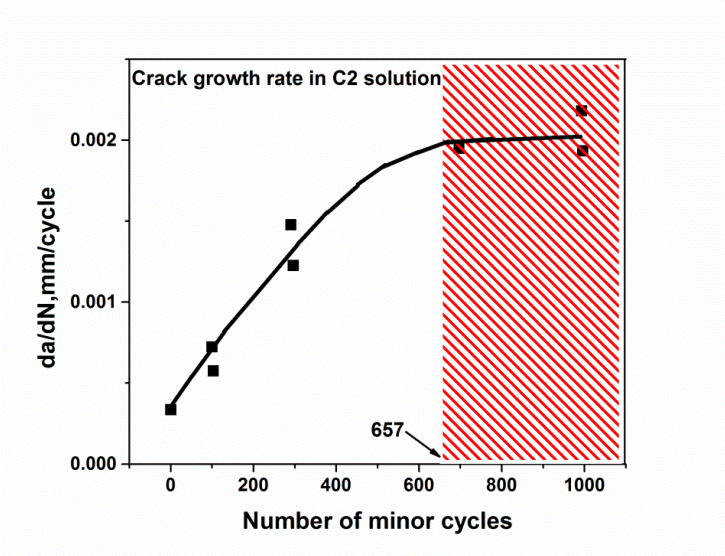

Figure 3.9 Crack propagation rate in terms of millimeter per block versus number of minor cycles. The shaded region is corresponding to the state, where hydrogen concentration in the plastic zone reaches saturated, leading to DTB transition and maximize crack propagation rate. To reach the state, the number of minor cycles should be larger than 657 by calculation, which is close to the experimental result, 697. [24]

The fracture morphologies displayed in Fig. 3.8 confirm the DTB transition along the cracking plane. If the number of minor cycles reaches 657, the plastic zone becomes

saturated and the crack growth rate is maximized. An increase in the number of minor cycles beyond this value will only make a small contribution to crack propagation based on Paris' law, $\left(da/dN\right) = C\Delta K^{m}$. But it will not enhance the hydrogen accumulation effect. Hence, there is a threshold for cracking rate $(da/dN)_{block}$, as the number of minor cycles *n* in each block reaches this value. Fig. 3.9 shows the number of minor cycles corresponding to the threshold detected in laboratory tests, which agrees with our theoretical prediction.

Table 3.1 The crack growth rate per block versus number of minor cycles [24]

Number of minor cycles per block, n	Measured crack growth rate (mm/block)
1	3.44E-04
1	3.20E-04
10	3.35E-04
100	7.09E-04
100	5.81E-04
300	1.24E-03
300	1.44E-03
697	1.92E-03
1000	2.10E-03
1000	1.96E-03

3.4 Conclusion

In this study, we firstly perform MD simulations to determine the free surface energy and stacking fault energy as a function of H concentration. Two ductile orientations, $\left[\bar{1}10\right](111)$ and $\left[001\right]\left(\bar{1}10\right)$, of cracks in α-iron were tested, as hydrogen atoms were introduced into the tetrahedral sites of a cubic bcc model. The simulations show that hydrogen embrittlement effects depend on the crack orientations. In orientation I, the hydrogen atoms enhance the

emission of dislocations by decreasing the stacking fault energy. It also enhance crack cleavage by decreasing the free surface energy. However, the changing rate of free surface energy versus the increasing hydrogen concentration is much faster than that of the stacking fault energy. Therefore, there is a cross-over of K_I^c and K_I^e as hydrogen concentration reaches a critical value, and cracks propagate before dislocations emit. In orientation II, hydrogen atoms increase the stacking fault energy as well as decrease the free surface energy. At the critical value of hydrogen concentration, K_I^c becomes smaller than K_I^e and the crack becomes brittle. Regardless of the orientation, hydrogen embrittlement effects can be expressed as a transition from ductile to "brittle".

The critical hydrogen concentration which is estimated from Mode I loading simulations can be applied to calculate the number of hydrogen atoms required to saturate the plastic zone under specific K_{max}, $\triangle K$, loading frequency and in a specific steel (corresponding to specific σ_{ys}). If cyclic loading is applied to a specimen, the hydrogen atoms accumulate in the plastic zone during cyclic loading and induce a DTB transition. We examined the number of minor cycles required to make this transition occur using the stochastic procedures described above. The calculated value is consistent with experimental tests and confirms our conclusion that DTB transition, which is enhanced by hydrogen accumulation, is not only related to the hydrogen concentration, but also the pressure fluctuations generated by the loading spectrum. Therefore, the model validated in this paper can be further developed to predict the long-ignored hazard pressure fluctuations in routine operations, such as minor cycles, and it can help to prolong the life of steel.

Chapter IV Atomistic study of hydrogen embrittlement during cyclic loading: quantitative model of hydrogen accumulation effects

4.1 Introduction

The fatigue behavior of metallic materials is an important issue in fracture mechanics. Near neutral pH stress corrosion cracking, which is a combination of corrosion and fatigue failure, is recognized as one of the most severe degradation mechanism in pipeline steel and cause tremendous losses in North America [32,100,102,103]. Many mechanisms have been proposed to illustrate the hydrogen induced ductility loss of steel (hydrogen embrittlement), including high hydrogen pressure bubble[104][7][105], hydrogen induced reduction in cohesive strength [hydrogen enhanced decohesion (HEDE)] [11,40,78,79,106], hydrogen enhanced local plasticity (HELP) [6,11,20,26,107], and hydrogen assisted vacancy production[107][108][109]. In general, the presence of atomic hydrogen in steel intends to enhance crack propagation. Current research also implies that hydrogen atoms have more significant effects on crack propagation as cyclic pressure fluctuations are applied to the steel [22,33,97]. Hence, hydrogen embrittlement is not only an issue of hydrogen effect on material, but also a matter of the loading condition. For instance, hydrogen diffusivity increases as steel is subjected to tension, and a bigger strain is beneficial for hydrogen charge. Molecular dynamics (MD) [110,111] with advanced characterization methods can help in uncovering atomic level mechanisms of hydrogen movement and crack advancement. MD simulation can reproduce phase transformations, twinning and dislocation generation processes which can be commonly observed in experiments [18,107]. In particular, the diffusivity of hydrogen atoms in steel lattice can be estimated and hydrogen

movement in steel can be quantified, which is non-trivial in experiments. Recently, predictive nano-scale mechanisms of HE have been quantified both for HEDE, in which the aggregation hydrogen atoms can induce a local "ductile to brittle" transition [28,29], and for HELP, in which hydrogen atoms form Cottrell atmospheres around moving dislocations and cause solute drag [22]. Unfortunately, all the nano-scale models developed so far are based on the single-static loading condition, however, hydrogen embrittlement has been proved to be not only related to hydrogen concentration, but also to the pressure fluctuations near crack tip [32,112]. Therefore, hydrogen embrittlement mechanism is necessary to put into a content of different loading spectra. In current work, we are aiming to reveal the atomistic mechanisms of hydrogen embrittlement in the most common pressure fluctuations in steel, such as in the minor cycles and unloading spectra [3,31].

Minor cycles ($K_{min}/K_{max} > 0.9$) are very common in the loading spectra of pipeline steels. However, based on the Paris law (i.e., $da/dN=c\Delta K^m$), the effects of minor cycles on crack propagation are expected to be negligible [85,113]. Recent experimental results have demonstrated that minor cycles, even with large R ratios as high as 0.9, can contribute to crack growth rate in underload spectrum [85]. Further investigations have shown that crack growth rate is dependent on the number of minor cycles and there is a threshold for the number of minor cycles that maximizes crack propagation in one loading block [85]. Since minor cycles can play a much more decisive role in NNpHSCC condition, it is natural to expect that minor cycles can accumulate hydrogen atoms and accelerate crack growth in hydrogen enhanced decohesion mechanism [29].

Crack propagation is not a continuous process during cyclic loading, and the loading rate and unloading rate both affect the crack growth rate. The current understanding is that increasing the loading rate or decreasing the unloading rate will enhance crack propagation. However, the atomistic crack growth mechanism and hydrogen diffusivity mechanism during cyclic loading still remain physically uncovered. In current study, MD simulations will be employed to study the propagation mechanism of single edge cracks and hydrogen accumulation mechanism of central cracks during cyclic loading where the R ratios of stress intensities range from 0.4 to 0.9. The simulation results clearly demonstrate the nature of discontinuous crack propagation during cyclic loading, and show the hydrogen accumulation near crack tip is linearly related to the number of minor cycles. Based upon these observations, a theoretical model was provided to quantify the hydrogen accumulation effects on crack growth in cyclic loading with minor cycles.

4.2 MD simulations in cyclic loadings

A single crystal bcc iron model is firstly constructed with crystallographic directions $\left[\bar{1}10\right]$ $\left[\bar{1}\bar{1}2\right]$ $\left[111\right]$ in the x, y and z directions, respectively. The simulation cell comprised of 420,000 Fe atoms is 40×2.1×60 nm along the x, y, and z directions. The crack is located in the middle of the z direction with [crack front direction](crack plane normal) $\left[\bar{1}10\right]\left(111\right)$. The initial crack length is about 100 Å and the width of the open mouth width is 20 Å. A typical model is shown in Fig. 4.1 (a) with free surface boundary condition along the x direction, periodic grain boundary condition along the y direction, and several fixed layers of atoms to apply displacement loading along the z direction to correspond to anisotropic elastic mode I stress intensity field K_I.

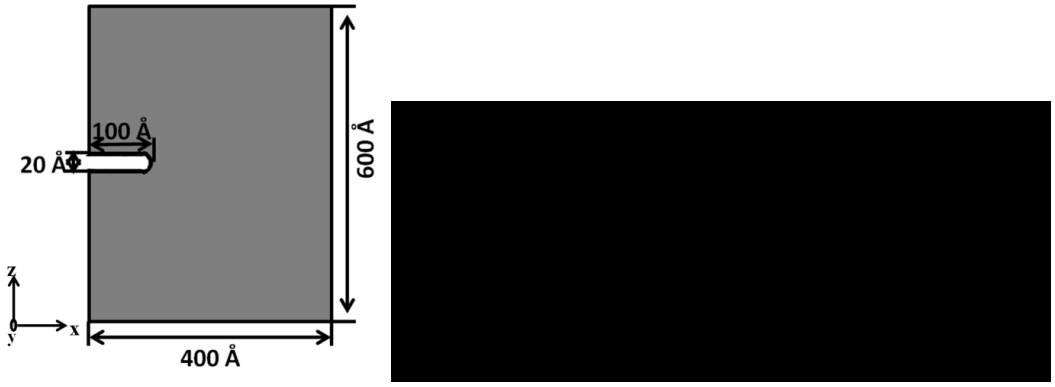

(a) (b)

Figure 4.1 (a) The geometry of the crack. (b) Loading spectra used in the simulation, where R $(K_{min}/K_{max}) = 0.4$.

MD simulations were performed using the microcanonical ensemble (NVT) [86] where the constant temperature is maintained by the Nose-Hoover method [87,88]. The atomic interactions are described with Embedded Atom Method (EAM) [89]. The potential is based on the Fe potential from Mendelev[24], and an extensive database of energies and atomic configurations from density functional theory (DFT) calculations have been derived from the cross interaction of H and Fe [59]. All simulations are carried out using LAMMPS [90]. Based on the literature survey, the hydrogen atoms would be stably located at the tetrahedral sites in BCC iron[27], and the distribution of hydrogen atoms will depend on hydrostatic stress. Hence, hydrogen atoms have been introduced into the model according to the following Eq. [4.1] [40].

$$c_{eq} = \begin{matrix} c_o \exp\left(\frac{4(1+v)K_I\Omega_H}{3\pi k_B T\sqrt{2\pi r}}\right), r \le r_o \\ c_o \exp\left(\frac{4(1+v)K_I\Omega_H}{3\pi k_B T\sqrt{2\pi r_o}}\right), r > r_o \end{matrix} \quad [4.1]$$

where c_o is the hydrogen concentration when stress = 0, v is Poison's ratio, Ω_H is the partial volume of hydrogen atom in BCC iron, k_B is the Boltzmann constant and T is the temperature. The model is initially loaded to K_I=0.8 MPa*m$^{0.5}$ which offers stress field for hydrogen accumulation. After the hydrogen atoms were introduced into the system according to hydrostatic stress, the systems were relaxed for 4 ns at T = 300 K. The further cyclic loading spectrums are shown in Fig. 4.1 (b). The maximum of loading stress intensity equals to 1.25 MPa*m$^{0.5}$. The propagation of cracks, the hydrogen distributions at the crack tips and stress distribution near crack are shown in Fig. 4.2. After four ns relaxation, the hydrogen atoms have accumulated at two sides in the crack front direction, as Fig. 4.2 (a) shows. The wedge-shaped H-rich region has induced extra tensile stress that makes the crack propagation easier. This was observed in previous work and was induced by the energy interaction of the H-Fe atoms' misfit and high tensile stress field [29]. Since the hydrogen concentration in the crack front is very high, the crack initiates in the first cycle of loading and continuously propagates during unloading in the second cycle, as Fig. 4.2 (b) shown. The stress field near crack tip during cyclic loading is always tensile. After the crack passes through the H-rich region, the crack becomes dormant and hydrogen atoms begin to accumulate in the crack front direction during unloading and loading sections because of tensile stress field, as Fig. 4.2 (c) and (d) shown. After the hydrogen cluster forms, hydrogen atoms will increase the local stress and diminish free surface energy [9], which enhance crack propagation. Because creating free surfaces will release the strain energy, the stress intensity will drop tremendously from 1.19 to 0.89 MPa*m$^{0.5}$ after crack growth, as (d) and (e) show.

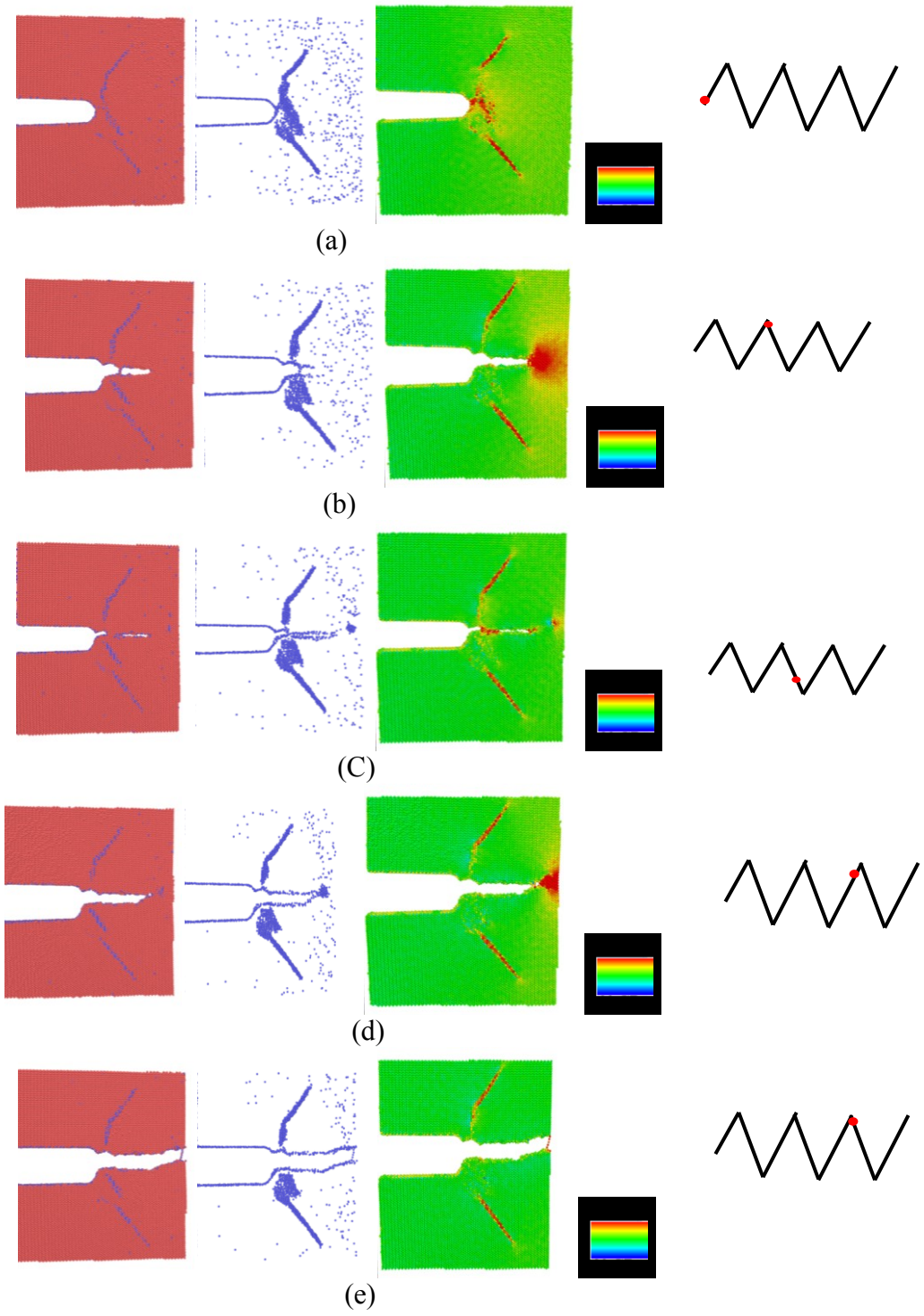

Figure 4.2 The crack tip geometry (first column), hydrogen distribution (second column), stress field distribution (third column) and loading spectrum (fourth column) under different stress intensity, as K_{max}=1.25 MPa*m$^{0.5}$ and R (K_{min}/K_{max}) = 0.4. Blue atoms are hydrogen

atoms and pink ones are iron atoms in crack tip geometry and hydrogen distribution figures. The corresponding stress intensity of each geometry is listed as follows, (a) K_I=0.8034 MPa*$m^{0.5}$; (b) K_I=1.25 MPa*$m^{0.5}$; (c) K_I=0.61 MPa*$m_0^{0.5}$; (d) K_I=1.19 MPa*$m_0^{0.5}$; (e) K_I=0.89 MPa*$m_0^{0.5}$.

The previous study suggests that the increase of hydrogen concentration will diminish the free surface energy; as a result, K_I^c values decreases [51]. During cyclic loading, as hydrogen-rich region forms, the stress intensity that requires to initiate crack propagation will be lower than that requires to induce crack-cleavage in air. The moving rate of hydrogen atoms should be related to hydrostatic stress distribution and the hydrogen concentration gradient. At the beginning of accumulation, hydrogen concentration is small and the hydrogen concentration's gradient can be neglected. The equation that could be used to predict the hydrogen movement velocity under this condition is described as Eq. [4.2],

$$V_r^{\sigma} = -\frac{D\Omega}{k_B T}\nabla\sigma^{hyd} = \frac{(1+v)\Omega}{k_B T 3\sqrt{2\pi}}\frac{DK_I\cos\frac{\theta}{2}}{r^{3/2}} \qquad [4.2]$$

where Θ is the angle between a line from specific position to crack tip and the crack front direction, and σ^{hyd} is the hydrostatic stress. However, if the hydrogen atoms have saturated the crack front direction and reach equilibrium, the reduction of hydrogen concentration along axial direction will drive the hydrogen atoms out and the concentration-related diffusion rate is shown as:

$$V_r^c = -D\nabla\ln\left(\frac{c}{1-c}\right) = \frac{-D}{c(1-c)}\nabla c = \frac{1}{1-c}V_r^{\sigma} \qquad [4.3]$$

where c is the hydrogen concentration near the plastic zone. The stress-driven H accumulation and the density gradient induced H diffusion will both occur as the hydrogen

concentration in the plastic zone is high. However, the V_r^c and V_r^σ would become comparable because the local hydrogen concentration c outside the plastic zone is low. It means that the trapped hydrogen atoms are difficult to move out and hydrogen atoms are forced to accumulate into plastic zone during cyclic loading, as illustrated in Figure 4.3.

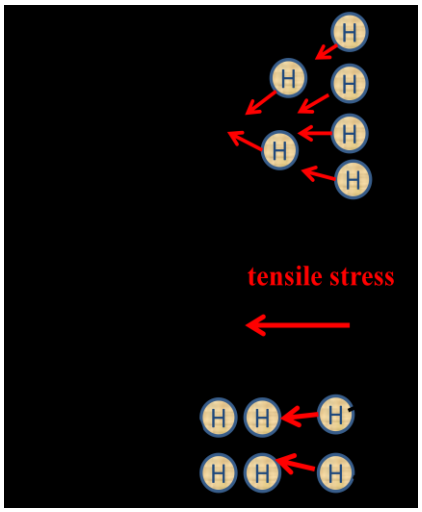

Figure 4.3 Competitive process of hydrogen accumulation as hydrogen concentration is low or high in the crack front direction.

4.3 MD simulations on minor cycles

The R=0.4 cyclic loading simulations verifies that hydrogen movement is asymmetric and hydrogen atoms are prone to accumulate into the plastic zone during cyclic loading. However, the crack growth rate in MD simulations is high, and the hydrogen-rich region is much easier to pass through as cracks begin to propagate. These simulations cannot be used to predict experimental tests or field operations due to the low loading rate. If the R ratio is increased to 0.9 (minor cycles), the cracks will stay dormant both in simulations and in experimental tests [85]. The minor cycles loading simulations may provide predictive capability in the way of hydrogen accumulation.

In order to reduce surface effect in x-direction (because of its tendency to segregate hydrogen atoms), the simulation model was modified to include a smaller central crack located at the center of X-Z surface [114]. A single crystal BCC iron model is constructed with crystallographic directions $[001][110]\left[\bar{1}10\right]$ in the x, y and z directions, respectively. The simulation cells comprised of 600,000 Fe atoms are 50×2.8×50 nm along the x, y, z directions. The initial crack length is about 50 Å and the width of the open mouth is 5 Å. A typical model is shown in Fig. 4.4 (a) with free surface boundary condition along the x direction, with periodic grain boundary condition along the y direction, and with several fixed layers of atoms to apply constant displacement loading along the z direction.

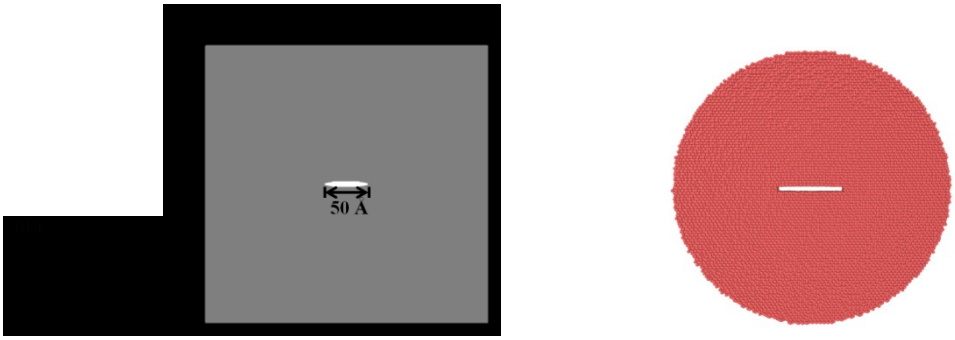

(a) (b)

Figure 4.4 (a) The geometry of the central crack model, (b) the initial size of the crack in a 10 nm curvature circular region.

The maximum stress intensity K_{max} is 0.65 MPa*m$^{0.5}$ and the R ratio of the minor cycles is 0.9 which ensures no crack propagation. The c_o is decided to be 0.001, which is ten times larger than the hydrogen concentration in steel under field operation [115]. The typical

model is firstly loaded to the maximum stress intensity. Hydrogen atoms are introduced into the model according to Eq. [4.1]. The hydrogen distribution and the geometry of the crack are shown in Fig. 4.5 (a). The hydrogen atoms will further diffuse to the central crack's free surfaces as Fig. 4.5 (b) shows. The maximum stress intensity for each minor cycle will stay the same around 0.65 MPa*$m^{0.5}$.

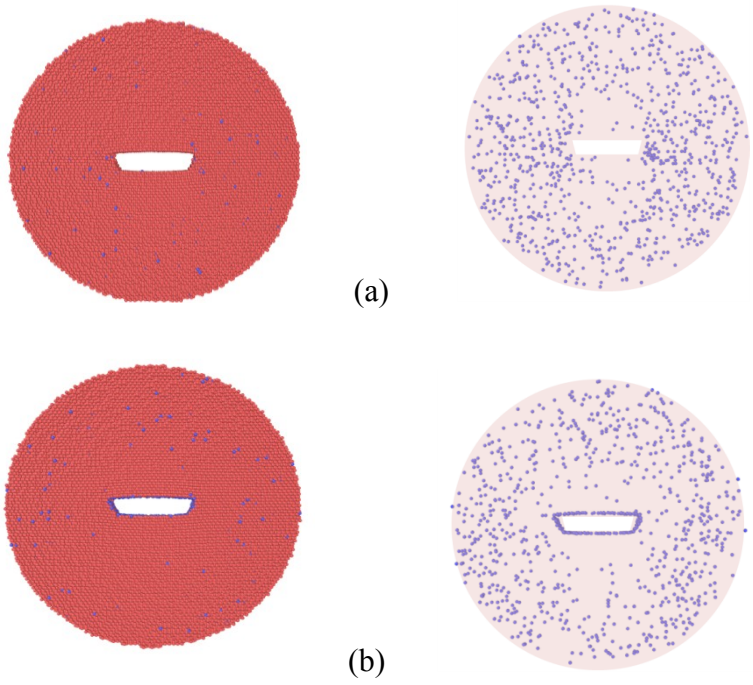

Figure 4.5 (a) Crack geometry after energy minimization, at first there are almost no hydrogen atoms on free surfaces; (b) hydrogen atoms' distribution after 2 minor cycles. There is no crack propagation or crack geometry change during minor cycles loading, and hydrogen atoms will saturate on the free surface.

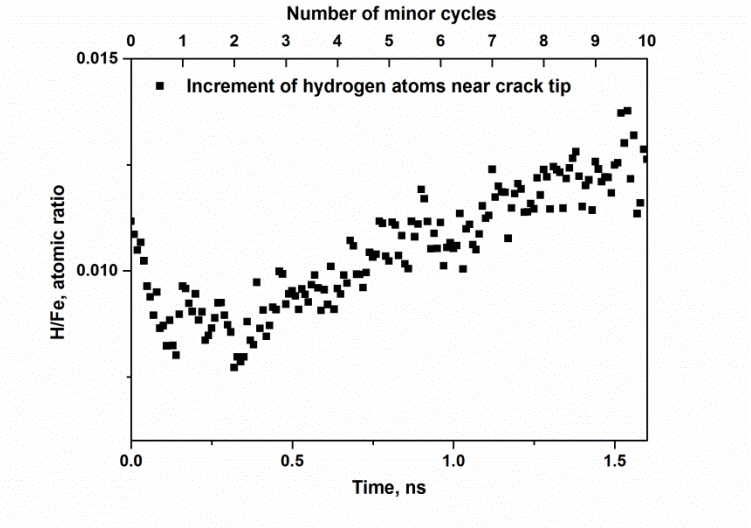

Figure 4.6 Hydrogen concentration in atomic ratio (H/Fe) near crack tip. There are ten minor cycles applied to the model. The initial two cycles will accumulate hydrogen atoms and most of them capture free surfaces. After that, the following cycles will continuously accumulate hydrogen atoms and the hydrogen concentration increased linearly.

The hydrogen atomic ratio around the crack in a circular region with the radius r = 10 nm is calculated, shown in Fig. 4.6. Only the hydrogen atoms in the body are considered and the ones on the free surfaces are neglected. Because the hydrogen atoms initially tend to diffuse to the free surfaces and saturate the surface area, there will be a drop of the H/Fe atomic ratio at the beginning of the loading. After the initial transition, the hydrogen concentration increases linearly with each increment of minor cycles. This linear relation can be described as,

$$n * \Delta c + c_o = c \qquad [4.4]$$

where n is the number of minor cycles, Δc is the hydrogen concentration increment, c_o is the original hydrogen concentration, and c is the hydrogen concentration after n minor cycles accumulation. In the experimental tests, it was observed a critical value of minor cycles that

maximizes the crack propagation and suggested that $c_{critical}$ should exist in Eq. [4.4], i.e., $n_{critical} * \Delta c + c_o = c_{critical}$. The $c_{ritical}$ corresponds to $n_{critical}$ which is a critical number of minor cycles and maximize the crack propagation in the hydrogen-assisted crack propagation mechanism. The crack growth model based on hydrogen-assisted decohesion mechanism can be shown as Eq. [4.5][97],

$$\left(\frac{da}{dN}\right)_{block} = \left[\frac{1}{\ln(1/c)}\right]^2 \frac{1}{\left(f_{critical}\right)^{0.1}} A(\Delta K, f, T) \qquad [4.5]$$

where c is $n * \frac{c_{critical} - c_o}{n_{critical}} + c_o$, $f_{critical}$ is the critical loading frequency, and A is the combined factor of loading. Since $c_{critical}$ is much larger than c_o, then Eq. [4.5] can be modified as,

$$\left(\frac{da}{dN}\right)_{block} = \left[\frac{1}{\ln\left(1/\left(n * \frac{c_{critical}}{n_{critical}} + c_o\right)\right)}\right]^2 \frac{1}{\left(f_{critical}\right)^{0.1}} A(\Delta K, f, T) \qquad [4.6]$$

If n is equal to zero, the crack growth rate in static loading is only related to c_o. The $c_{critical}$ is assumed to be the hydrogen concentration, which induces ductile-to-brittle transition and equals 280 ppm, based on our previous simulation [116]. The $n_{critical}$ can be estimated from equation

$$n_{critical} = \frac{\int_{K_{\min}}^{K_{\max}} \int_0^{r_p} 1.15 c_{critical} \exp\left(\frac{\sigma^{hyd}\Omega}{k_B T}\right) 2\pi r dr}{c_o[\pi(r_p + \bar{V}_r * t)^2 - \pi r_p^2]} \qquad [4.7]$$

where σ^{hyd} is hydrostatic stress near crack tip that is equal to $\sigma^{hyd}(r) = \frac{4(1+v)}{3\pi\sqrt{2\pi r}} K_I$, and $\bar{V}_r$ is the average velocity of hydrogen atoms that is equal to $\bar{V}_r = \frac{\int_{K_{\min}}^{K_{\max}} V_r(K_I, r_p)\, dK_I}{K_{\max} - K_{\min}}$. The

predicted value of n_{critical} is equal to 657, which is consistant with the experimental tests, 697 [85].

The minor cycles' acceleration factor can be quantified with a ratio of Eq. [4.6] divided by itself as n is equal to zero, or can be simplified as $\alpha_{\text{acceleration}}(n) = \left[\frac{\ln(1/c_o)}{\ln(\frac{n_{critical}}{nc_{critical}})} \right]^2$. The predicted acceleration factor is compared with the experimental tests and agree with each other quite well. When the number of minor cycles is smaller than the threshold, each increment of minor cycles will increase crack growth per block significantly. However, as n is above the threshold, crack growth rate will not be enhanced by further increment of n. This fact verifies that the enhancement of crack growth is induced by hydrogen accumulation of minor cycles. As the plastic zone is saturated, the further increment of minor cycles will only acuumulate more hydrogen, therefore, crack growth reaches maximum.

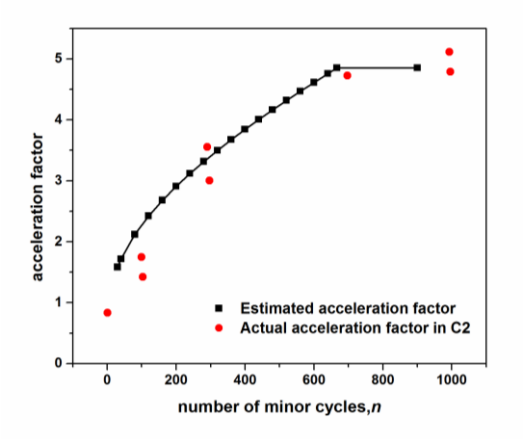

Figure 4.7 The estimated acceleration factor compared with the experimental factor in X-60 steel. Both reach the same threshold.

4.4 Conclusion

In current study, MD simulations show that hydrogen-assissted crack growth mechanism is an interaction of hydrogen atoms' effects on the behavior of metal and the pressure fluctuations effects on movement of hydrogen atoms. Cyclic loading has an effect on accumulating hydrogen atoms and make the planar fracture easily occur both in loading and unloading sections. After a crack propagates through the hydrogen-rich region, several cycles are required to accumulate enough hydrogen atoms. Hence, the crack propagation is not continuous. Minor cycles have no direct enhancement on crack growth; however, they have significant effects on accumulating hydrogen atoms and enchancing the crack growth. The predictive model of minor cycles' acceleration effect on crack growth agrees well with experimental tests.

The mechanism proposed and validated here is related to hydrogen enhanced decohesion. The interaction of hydrogen and cyclic loading effects is quantitatively descrived as a

mathematical model in current work and this model has been verified to have quantitative predictive capability. This model revealed the nature of hazard operating spectra such as minor cycles and can be used to modify the loading spectra in pipeline or other steels. This research will be helpful as a basis for other studies to prolong the life of steel.

Chapter V The effects of pressure fluctuations on hydrogen embrittlement in pipeline steels

5.1 Prediction of crack propagation under cyclic loading based on hydrogen diffusion

5.1.1 Introduction

Hydrogen embrittlement has been well accepted as one of the most severe steel degradation mechanisms [51,76,117,118]. There are several theories to illustrate hydrogen embrittlement in steel. Hydrogen Enhanced Local Plasticity (HELP)[119] postulates that hydrogen would not lock dislocations in place and instead it would enhance the movement of dislocations. The increased local plasticity is believed to cause an increase in local stress so that crack can be initiated easily [82,120]. Hydrogen Enhanced Decohesion (HEDE)[106,121] postulates that H atoms in steel would diminish the bonding energy between adjacent iron atoms and this mechanism causes an easier planar failure[122]. Lynch's theory which involves H promoting dislocation nucleation, and facilitating the link up of cracks with voids ahead of cracks is also reasonable in explaining material changing from ductile to brittle as H concentration increases[13].

This paper aims to build a theoretical model of crack propagation in pipelines based on current laboratory results and Paris law. According to Paris law, the crack growth rate is related to maximum loading stress intensity K_{max}, the range of loading stress intensity ΔK and loading frequency f [12]. However laboratory tests in NNpHSCC find that the cracking rate remains constant below a specific loading frequency. This loading frequency has been

A version of section 5.1 in this chapter has been published: X. Xing, et al. Mater. Lett. 152 (2015) 86–89.

defined as a critical loading frequency f_{critical} [32]. Since previous studies suggested that hydrogen distribution is dependent on hydrostatic stress [91][40] and hydrogen movement is dependent on stress intensity [28], it is reasonable to conclude that f_{critical} should be related to hydrogen diffusion and should depend on fracture mechanics and hydrostatic stress. A crack propagation model based on hydrogen diffusion can be rewritten as follows:

$$\left(\frac{da}{dN}\right)_{tot} = \left(\frac{f_{critical}}{f}\right)^{\gamma} \left(\frac{da}{dN}\right)_{HAC}^{max} \qquad [5.1]$$

where $(da/dN)_{HAC}$ is the crack propagation rate due to hydrogen-assisted cracking. The $(da/dN)_{HAC}$ term takes into account both the HEDE theory and Lynch's theory, where the former expects the accumulation of H at the crack front direction to diminish the free surface energy and cause crack propagation [29,101] and the latter considers the coalescence of the minor defects with cracks due to H effects [16,23,109]. As hydrogen atoms saturate in the plastic zone, two mechanisms will enhance the crack propagation rate to reach the maximum rate, as suggested by the recent experiments [32]. Since both mechanisms are related to hydrogen diffusion, the total hydrogen-assisted cracking rate is naturally expected to have a power law relationship with the cracking propagation rate based on HEDE. Hence, the main task in this model is to develop the crack propagation rate based on the HEDE mechanism.

5.1.2 Cracking model based on hydrogen diffusion

Based on the equilibrium condition, the hydrogen concentration near the crack tip is related to the hydrostatic stress distribution [74,75] and can be expressed as:

$$c = c_o \exp\left(\frac{\sigma^{hyd}\Omega}{k_B T}\right) \qquad [5.2]$$

where c_0 is the atomic ratio of *H/Fe* away from the crack tip, Ω is the partial volume of hydrogen, k_B is the Boltzmann constant, and σ^{hyd} is the hydrostatic stress which is shown as:

$$\sigma^{hyd}(r,\theta)=\frac{1}{3}\left(\sigma_{xx}+\sigma_{yy}+\sigma_{zz}\right)=\frac{2(1+v)}{3\sqrt{2\pi r}}K_I cos\frac{\theta}{2} \quad [5.3]$$

where v is Poisson's ratio, K_I is stress intensity, r is the distance from any specific position to the crack tip, and Θ is the angle between the crack front direction and the line from the specific position to the crack tip. Here we employ the criteria that when the atomic ratio reaches 1, the free surface forms and the crack propagates [22,28]. Hence, the length of the saturated zone can be estimated as:

$$L(K_I)=\left[\frac{4(1+v)\Omega}{3\pi k_B T\sqrt{2\pi}ln\left(\frac{1}{c_0}\right)}\right]^2 K_I^2 \quad [5.4]$$

Therefore, the maximum $(da/dN)_{HEDE}$ is the difference of $L(K_I)$ as K_I changes from K_{min} to K_{max} and the value can be shown as:

$$\left(\frac{da}{dN}\right)_{HEDE}^{max}=L_{max}-L_{min}=\left[\frac{4(1+v)\Omega}{3\pi k_B T\sqrt{2\pi}ln\left(\frac{1}{c_0}\right)}\right]^2\left(\frac{1+R}{1-R}\right)\Delta K^2 \quad [5.5]$$

where $L_{\min}$ is the saturated length at K_{min}, $L_{\max}$ is the saturated length at K_{max}, and the R ratio is equal to K_{min}/K_{max}. The $(da/dN)_{HEDE}$ is the crack propagation rate related to hydrogen diffusion. When $f < f_{\text{critical}}$, the $da/dN = (da/dN)_{max}$, however, when $f > f_{\text{critical}}$, the da/dN value will vary with loading frequency, i.e.:

$$\left(\frac{da}{dN}\right)_{HEDE}=\left(\frac{da}{dN}\right)_{HEDE}^{\max}\left(\frac{f_{critical}}{f}\right)^{\gamma} \quad [5.6]$$

The power of loading frequency Υ can be fitted from experimental results, which are expected to be related to hydrogen diffusion. The hydrogen concentration in the steel is difficult to quantify and could range from 0 to $5*10^{-4}$ atomic ratio [40]. To simplify the

calculation, the c_0 here is taking a constant at 2 ppm, which is a reasonable amount around crack tips in steel [29,101].

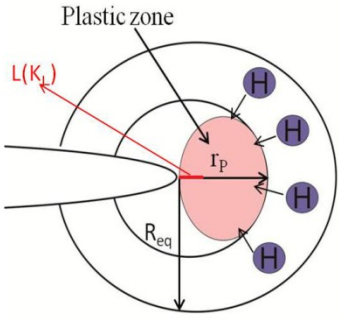

Figure 5.1 The schematic of the H enhanced crack propagation model. The pink region is the plastic zone, in which the size is equal to r_p. The annulus region in which the inner radius equals r_p and the outer radius equals R_{eq} is the zone that supplies and depletes hydrogen atoms to and from the plastic zone during cyclic loading. $L(K_I)$ is the length of a free surface (the distance that the crack propagates) covered by hydrogen atoms.

The plastic zone shape under the plain strain condition can be approximated to be a circular region with a radius r_p as shown in Fig. 5.1, which is reasonable because when the H concentration in the circular region reaches equilibrium, its concentration in the plastic zone also reaches saturation. To reach the dynamic equilibrium of hydrogen concentration in the plastic zone during cyclic loading, an annulus region with the inner radius r_p and the outer radius R_{eq} is needed to supply and deplete hydrogen atoms. The hydrogen concentration outside of the plastic zone is estimated to be c_0. Therefore, the minimum time, $t_{critical}$, needed for H diffusion in/out of the circular region during the cyclic load to satisfy the dynamic equilibrium hydrogen concentration in the plastic zone is related to the critical frequency

through $f_{critical}=1/(2t_{critical})$. Hence, the number of hydrogen atoms needed to saturate the plastic zone can be calculated as follows:

$$N(K_I)=\int_{L(K_I)}^{r_p}\frac{c_o\exp\left(\frac{\sigma^{hyd}\Omega}{k_BT}\right)2\pi r l_z}{a_o^3/2}dr+\frac{4L(K_I)^2 l_z}{a_o^3} \quad [5.7]$$

where r_p is the plastic zone size based on plain strain condition $\frac{1}{6\pi}\left(\frac{K_{\max}}{\sigma_{ys}}\right)^2$, a_0 is the lattice parameter, l_z is the thickness of the specimen and $L(K_I)$ is the free surface length where hydrogen concentration is equal to one. As K_I changes from K_{min} to K_{max}, the hydrogen numbers change in the circular region in which the radius r_p is $N(K_{max})$-$N(K_{min})$. This difference could be calculated by changing K_I in Eq. [5.7] from K_{min} to K_{max}. The exchanging of H atoms in the plastic zone then be supplied to or depleted by an annulus region in which the inner radius equaled r_p and the outer radius equaled R_{eq}. Hence, the increase of H atoms in the plastic zone during one single cycle of loading should still be equal to the H numbers in this annulus region as Eq. [5.8] shows.

$$N(K_{\max})-N(K_{\min})=\frac{2\pi c_o l_z}{a_o^3}\left(R_{eq}-r_p\right)^2 \quad [5.8]$$

The average velocity of the hydrogen movement $\overline{V}_r$ over position and stress intensity can be estimated from the hydrogen chemical potential deduced force and the motivation [29,50]. The hydrogen chemical potential can be shown as:

$$\mu=\mu_o+k_BT\ln\frac{c}{1-c}+\sigma^{hyd}\Omega \quad [5.9]$$

and the velocity can be expressed as:

$$V_r=\frac{DF_r}{k_BT}=\frac{(1+\nu)\Omega}{k_BT3\sqrt{2\pi}}\frac{DK_I\cos\frac{\theta}{2}}{r^{3/2}} \quad [5.10]$$

As hydrogen atoms flux into the plastic zone during loading, the hydrogen concentration outside the plastic zone is assumed to be a constant c_o, hence $F_r = -\nabla\mu = -\Omega\nabla\sigma^{hyd}$. Then the average velocity is:

$$\overline{V}_r = \frac{\int_{r_p}^{R_{eq}}\int_0^{\pi}\int_{K_{min}}^{K_{max}} V_r dK_I d\theta dr}{\pi\left(R_{eq}-r_p\right)\left(K_{max}-K_{min}\right)} \qquad [5.11]$$

The $t_{critical}$ value is equal to the size of the zone which supplies or depletes the hydrogen atoms over the average velocity, i.e., $f_{critical} = \frac{1}{2t_{critical}}$, then:

$$f_{critical} = \frac{(1+v)\Omega D\left(K_{max}+K_{min}\right)\left(\frac{1}{\sqrt{r_p}}-\frac{1}{\sqrt{R_{eq}}}\right)}{\pi\left(R_{eq}-r_p\right)^2 k_B T 3\sqrt{2\pi}} \qquad [5.12]$$

In Eq. [5.12], the $f_{critical}$ is proportional to hydrogen diffusivity, and D is about $2*10^{-11}$ m^2/s [80] when the strain of the specimen is equal to zero. However, molecular dynamics (MD) simulation shows that there is an excess volume for hydrogen atoms as the specimen is under tensile strain. Hence, the diffusivity of hydrogen can be almost two orders higher than that value and can reach $1.7*10^{-9}$ m^2/s [48]. Therefore, this D value is used in the current calculation and the HEDE propagation rate can be shown as:

$$\left(\frac{da}{dN}\right)_{HEDE} = \left[\frac{4(1+v)\Omega}{3\pi k_B T\sqrt{2\pi}\,ln\left(\frac{1}{c_0}\right)}\right]^2 \left(\frac{1+R}{1-R}\right)\frac{\Delta K^2}{\left(f/f_{critical}\right)^{\gamma}}, f > f_{critical} \qquad [5.13]$$

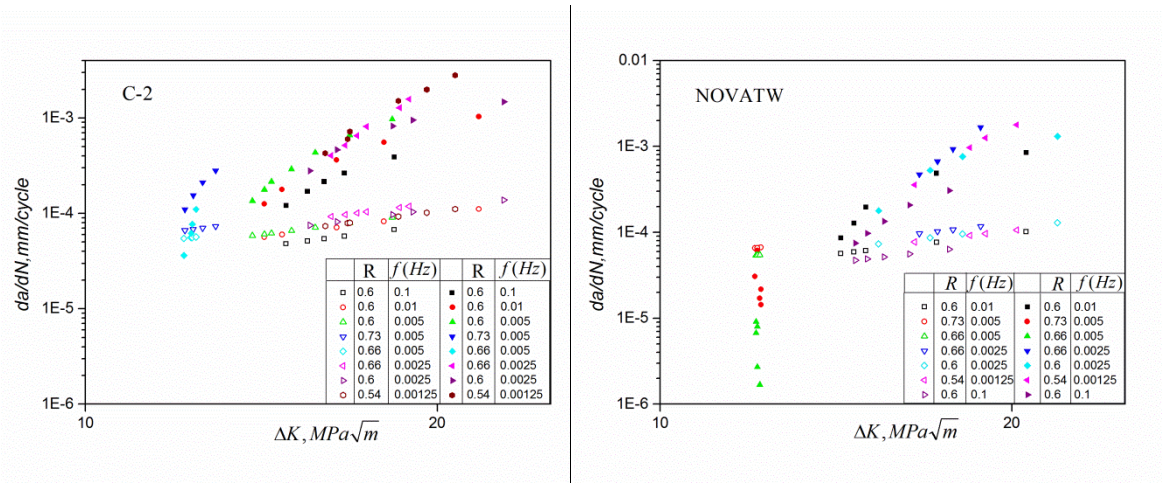

(a) (b)

Figure 5.2 (a) A comparison of the experimental measured crack propagation rate and the calculated rate using Eq. [5.13] in C-2 solution, and (b) a comparison of the experimental measured crack propagation rate and the calculated rate using Eq. [5.13] in NOVATW solution. The (da/dN)tot (solid symbols) show a stronger ΔK dependence compared with the calculated (da/dN)HEDE (open symbols). [33][123]

Fig. 5.2 compares the estimated HEDE crack growth rates with experimental results in C-2 and NOVATW solutions [33]. The hollow symbols (HEDE) and the solid symbols (experimental values) have the same trend. The predicted HEDE crack propagation rate and the total crack propagation rate from experiments both show a power law with $\triangle K$. This suggests that the estimated HEDE propagation rate based on hydrogen diffusion and critical loading frequency could be related to the Paris Law and could provide physical meaning for this empirical model in NNpHSCC. The deviation of slop in predicting the HEDE propagation rate is proportional to the deviation of the experimental crack propagation results. This relationship can be simply related by a power law:

$$\log\left(\frac{da}{dN}\right)_{tot} \Big/ \log\left(\frac{da}{dN}\right)_{HEDE} = n \qquad [5.14]$$

where n is the constant for specific steel. Hence, the overall crack propagation rate should be proportional to the stress intensity and frequency as Eq. [5.15] shows:

$$\left(\frac{da}{dN}\right)_{tot} = \left[\frac{4(1+\nu)\Omega}{3\pi k_B T\sqrt{2\pi}\, ln\left(\frac{1}{c_0}\right)}\right]^{2n} \left(\left(\frac{1+R}{1-R}\right)\frac{\Delta K^2}{\left(f/f_{critical}\right)^{\gamma}}\right)^{n}, f > f_{critical} \qquad [5.15]$$

Therefore, a new crack propagation model in the form of the Paris Law can be simplified as:

$$\left(\frac{da}{dN}\right)_{tot} = A\left(\left(\frac{1+R}{1-R}\right)\frac{\Delta K^2}{\left(f/f_{critical}\right)^{\gamma}}\right)^{n}, f > f_{critical} \qquad [5.16]$$

where A and n are constants and A is proportional to $1/T$ and ln ($1/c_0$). The term $\left(\frac{1+R}{1-R}\right)\frac{\Delta K^2}{\left(f/f_{critical}\right)^{\gamma}}$ is a combined factor of loading and hydrogen diffusion, and the γ value can be fitted from experimental results. Figure 5.3 shows a crack propagation rate of X-65 steel in C-2 and NOVATW solution [33] in NNpHSCC and X52 steel in C2 solution [123] in terms of the new combined factor, where we take γ as 0.1 and all the data show reasonable convergence.

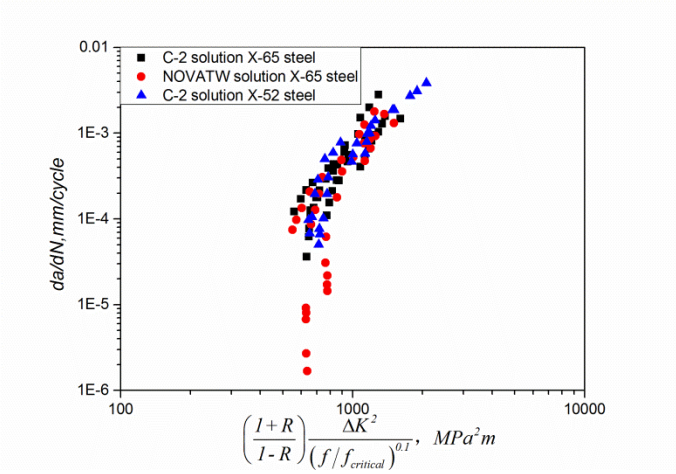

Figure 5.3 The combined factor fits with the crack length from experimental results. All of the cracking rate data in different loading frequencies and stress ratios fit very well with the single Υ value, 0.1. [33][123]

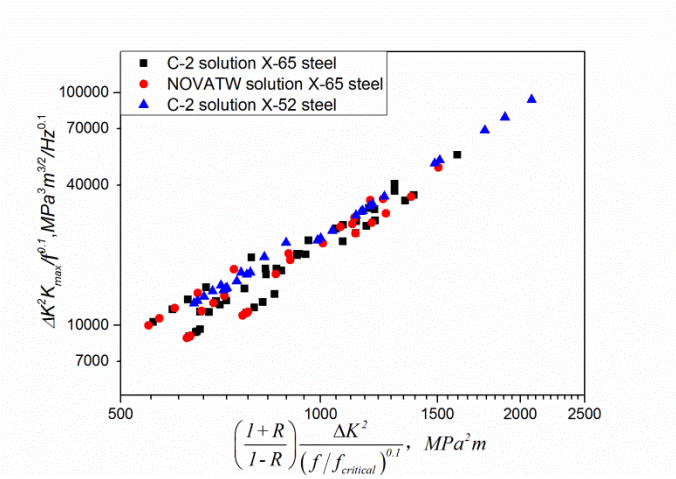

Figure 5.4 The correlation between the two combined factors based on the empirical model in the previous study and the theoretical prediction on hydrogen diffusion.

In Fig. 5.4, we plot the combined factor $\left(\frac{1+R}{1-R}\right)\frac{\Delta K^2}{(f/f_{critical})^{0.1}}$ based on current model against the previous combined factor $\frac{\Delta K^2 K_{\max}}{f^{0.1}}$, which was successfully used to predict the durability of pipeline steel [33]. The power law relationship between the two combined factors suggests they are correlated and that both are based on the same mechanism.

5.1.3 Conclusion

The new model, which includes a hydrogen accumulation factor, can be used to predict crack growth and rationalize the model based on X-65 steel experimental tests. Furthermore, it can be used to predict the crack propagation rate in other steels with fitted *A* and *n* values in equations. The crack propagation rate can be easily correlated to a combined factor $\left(\frac{1+R}{1-R}\right)\frac{\Delta K^2}{(f/f_{critical})^{0.1}}$. This factor has combined the hydrogen diffusion, critical loading frequency, and cyclic loading. It has a power law relationship with the previous combined factor $\frac{\Delta K^2 K_{\max}}{f^{0.1}}$, suggesting that both factors are based on the same mechanism. Therefore, current study provides a strong theoretical foundation for the Paris Law and previous empirical model in the NNpHSCC.

5.2 Application of the crack model

The mechanisms for crack growth in pipeline steel of different loading spectra such as overloading and minor cycles are well established. However, if hydrogen atoms were introduced into a specimen, these mechanisms may not work because of hydrogen asymmetric diffusion during cyclic loading. In our assessments, hydrogen atoms will accumulate into the plastic zone in each cycle of loading because of hydrostatic stress distribution and the hydrogen concentration gradient [28]. This hydrogen accumulation effect will enhance the crack propagation of pipeline steel, notably in near neutral pH stress corrosion cracking (NNpHSCC).

Overloading has a retardation effect for crack propagation in air, and the mechanisms can be clarified as follows: 1. The overloading blunts the crack tip and further resharpening of crack tip needs more time, 2. Compressive residual stress in the front of crack tip caused by overload retards the crack growth, 3. Residual stress behind the crack tip leads to plasticity-induced closure [124–127]. However, overloading introduces a cycle with bigger ΔK and K_{max} into the loading spectra, which will induce initial crack growth acceleration and enhance in hydrogen accumulation. The accumulated hydrogen atoms can enhance the crack propagation and might be able to eliminate the aforementioned retardation effects.

The same scenarios can occur in spectra containing minor cycles. Since the R (K_{min}/K_{max}) ratio of minor cycles is very large, the Paris model predicted that minor cycles could only make small contributions to crack propagation. Some laboratory results also show that there is a threshold of ΔK, below which the crack growth rate will drop to zero [33]. However, current studies in NNpHSCC have shown that compared to tests without minor cycles, there

A version of section 5.2 in this chapter has been published: X. Xing, et al. IPC 2016-64478.

is an increase in the crack growth rate by a factor of 3 to 5 as some minor cycles are added to the underloading spectra [85]. Compared with underloading, a single minor cycle cannot significantly accelerate crack growth. However, a significant number of minor cycles can gather hydrogen atoms and change cracks from ductile to brittle as the hydrogen concentration increased in the crack front direction. These aggregated hydrogen atoms highlight the role of minor cycles in crack growth. A new model has been developed to predict crack propagation rate based on the HEDE mechanism. Afterward, the new model combined with the hydrogen accumulation theory can be used to quantify hydrogen effects in the crack growth of overload and minor cycles.

5.2.1 Overloading retardation

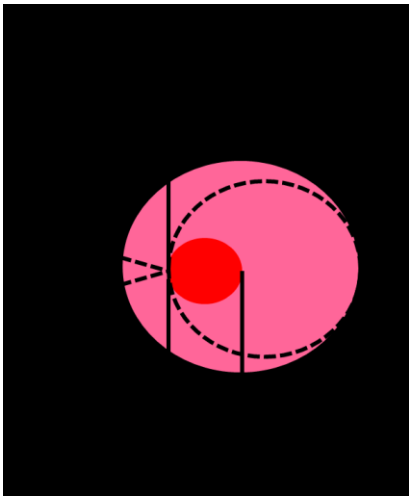

Figure 5.5 The schematic of the overloading plastic zone. The red region is the plastic zone produced by the i cycle of constant loading, in which the size is equal to r_{pi}. The pink region is the plastic zone produced by overloading, in which the size is equal to r_o.

The overloading retardation effect in the current model can be approximated by a ratio of two f_{ciritial} values which are related to the plastic zone created by the constant loading $K_{\max}$ and overloading $K_{\max}{}^{o}$. The overloading retardation is dependent on plastic deformation and tensile stress in the plastic zone as the specimen is loaded in the air. However, the hydrogen accumulation in the crack tip will also be contributing to crack propagation as the specimen is loaded under NNpHSCC conditions. The retardation factor is shown below

$$\phi_{rH} = \left(\frac{f_{critical}^{\text{constrainzone}}}{f_{critical}^{\text{loadingzone}}} \right)^{0.15} = \left(\frac{(\mathrm{R}_{eqi} - r_{pi})^2 \left(\frac{1}{\sqrt{r_o - \Delta a}} - \frac{1}{\sqrt{R_{eq}^*}} \right)}{(\mathrm{R}_{eq}^* - r_o + \Delta \mathrm{a})^2 \left(\frac{1}{\sqrt{r_{pi}}} - \frac{1}{\sqrt{R_{eqi}}} \right)} \right)^{0.15} \qquad [5.17]$$

where r_{pi} is the size of the plastic zone produced by the i cycle of constant loading, r_{o} is the plastic zone created by overload, and Δa is the crack length change. The constraint zone size is the difference of r_{o} and Δa, and R_{eq}-r_{p} is the size of an annulus region that depletes and offers hydrogen atoms to the plastic zone and can be calculated with Eq. [5.8].

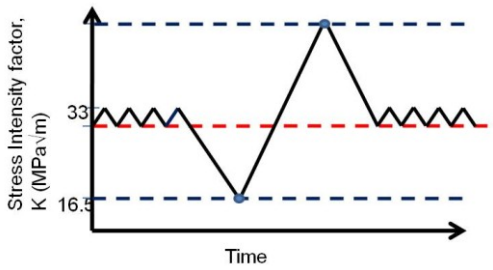

(a)

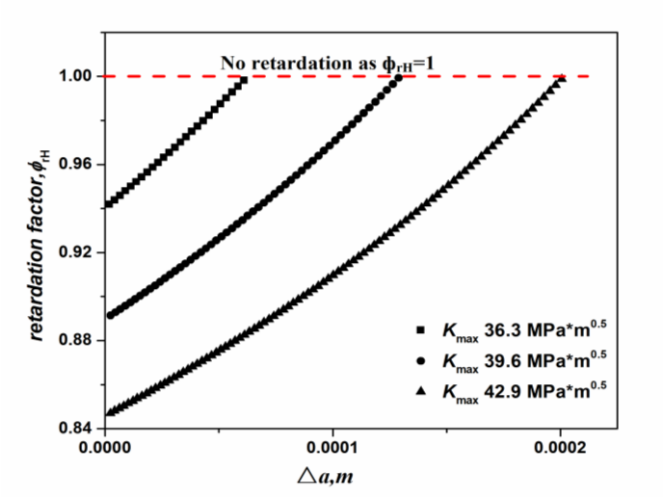

(b)

Figure 5.6 (a) Variable amplitude waveform: K_{min}=16.5 MPa*$m^{0.5}$, K_{max} for constant loading is 33MPa*$m^{0.5}$ and the R ratio of minor cycles is equal to 0.9. (b) A comparison of the predicted overloading retardation factor for 10%, 20% and 30% overloading with Eq. (17).

As Fig. 5.6 shows, overloading has a beneficial effect in retarding crack propagation as ϕ_{rh} is smaller than one. A larger K_{max} in overload will generate a larger plastic zone, and more hydrogen atoms should be needed to saturate the plastic zone before the hydrogen atoms could diffuse to the crack front direction. As cracks propagate to a position where the constant loading plastic zone can exceed the boundary of the overloading plastic zone, the retardation effects will be removed and ϕ_{rh} will return to one.

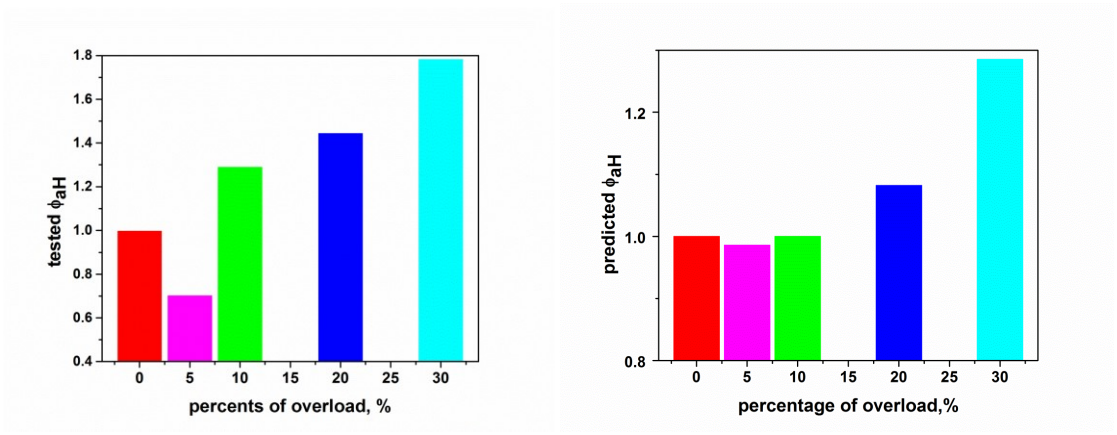

(a) (b)

Figure 5.7 (a) A comparison of experimental acceleration factors for different overload ratios ranging from 0%~30%; (b) A comparison of predicted acceleration factors for different overload ratios ranging from 0%~30%;

Experimental tests in C2 solution shows that as the K_{max} of overloading increases, the crack propagation accelerates. Fig. 5.7 shows a comparison of the acceleration factors for different ratios of overloading. In particular, 30% overloading does not lead to a larger retardation factor than 10% overloading. The acceleration may be attributed to the initial overloading acceleration. If neglecting the crack propagation of the minor cycles, the crack growth rate of each block is divided into two parts: crack growth during underload and crack growth during overload. The crack growth rate has a relation with the range of stress intensity which is roughly expressed as $(da/dN) \sim \Delta K^3$. Hence the acceleration factor of overload can be described as follows

$$\phi_{aH} = \frac{\phi_{rH}\left(n_1 \Delta K_{underload}^3 + n_2 \Delta K_{overload}^3\right)}{n_1 \Delta K_{underload}^3} \qquad [5.18]$$

where n_1 is the number of underload cycle in each block and n_2 is the number of overload cycle in each block. The predicted values show good convergence with laboratory tests. As overload ratio is near 5%, the initial overload acceleration is very small. However, 5% overloading bring in significant retardation effect because of the plastic zone size change. As overloading is increased, the overload acceleration overcome it's retardation effects and enhance crack growth.

5.2.2 Minor cycle acceleration

Based on current experimental results, there is a critical number of minor cycles which maximizes the crack growth rate for the underload spectrum [85]. This critical value can be assessed based on the following arguments: 1) an equilibrium hydrogen concentration (maximum) could maximize crack propagation and saturate the plastic zone; and 2) minor cycles affect the accumulation of hydrogen atoms. Furthermore, the critical number of cycles is equal to the number of hydrogen atoms required to saturate the crack tip divided by the number of hydrogen atoms that can be accumulated at the tip in each minor cycle. The loading spectrum is shown in Fig. 5.8, where K_{max} is equal to 33 MPa$\sqrt{m}$, the R ratio of the underload is 0.5, the the R ratio of minor cycles is 0.9 and n is the number of minor cycles in each block.

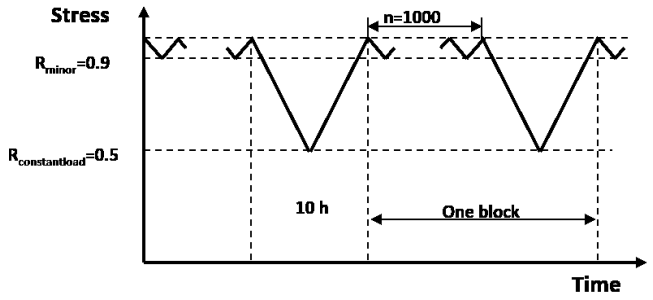

Figure 5.8 Variable amplitude waveform: K_{max}=33 MPa*$m^{0.5}$, the R ratio of minor cycles=0.9, the R ratio of underload=0.5, the frequency of minor cycles=0.00538 Hz, the frequency of underload=0.0000278 Hz (10 h/cycle), the number of minor cycles per block n =1000.

There is a theoretical hydrogen concentration outside the plastic zone which can affirm the ductile-to-brittle transition in mode I loading. This value has been estimated using the MD simulations and is equal to 280 ppm [116]. The number of hydrogen atoms needed to saturate the plastic zone could be calculated using the equation shown below:

$$N_H^{total} = \frac{c_{critical} B[\pi(r_p + \bar{V}_r * t_{critical})^2 - \pi r_p^2]}{a_o^3/2}, \quad \text{where } \bar{V}_r = \frac{\int_{K_{min}}^{K_{max}} V_r(K_I, r_p)\, dK_I}{K_{max} - K_{min}} \qquad [5.19]$$

$\bar{V}_r$ is the average moving velocity of hydrogen atoms at $r = r_p$ as stress intensity ranges from K_{min} to K_{max}. A linear summation of the crack growth rates of each cycle with the Paris Law is the most common method to calculate the crack growth rate. Although each minor cycle can only make a small contribution to crack growth, a significant number of minor cycles have effects in accumulating hydrogen atoms and only generate a small distance of free surfaces. Hydrogen atoms diffusing out from these free surfaces can be neglected unlike those accumulating into the plastic zone. If minor cycles accumulate enough hydrogen atoms

and saturate the plastic zone, the crack growth rate will be maximized. Hence, the number of minor cycles needed to saturate the plastic zone is equal to $\frac{N_H^{total}}{N_H^{\min orcycle}}$.

The theoretical value of minor cycles needed to maximize the crack propgation is equal to 676 cycles, which is consistent with the laboratory tests shown in Fig. 5.9. The correlation of the theoretical hydrogen accumulation model and experimental results verifies the minor cycles' effect in accelerating crack propagation in NNpHSCC. Hence, an accelerating factor should be added to modify the Paris model [74][128] when minor cycles exist in the loading block. In a theoretical model, the crack growth rate is expresssed in a relationship with the hydrogen concentration as Eq. [5.20] shows:

$$\left(\frac{da}{dN}\right)_{constload} = \left[\frac{1}{\ln(1/c_o)}\right]^2 \frac{1}{(f_{critical})^{0.1}} A(\Delta K, f, T) \qquad [5.20]$$

As c_o becomes larger, the crack propagation rate is enhanced. Furthermore, if c_o can reach the theoretical critical concentration, the crack propagation rate should be maximized. The c_o is a constant and will not change with increments of minor cycles. However, each increment of minor cycles will increase the number of hydrogen atoms that accumulate into the plastic zone, generating the same effects as each increment of c_o. The crack growth rate for one block with n minor cycles can be estimated with the following equation:

$$\left(\frac{da}{dN}\right)_{ncycles} = \left[\frac{1}{\ln(\frac{n_{critical}}{nc_{critical}})}\right]^2 \frac{1}{(f_{critical})^{0.1}} A(\Delta K, f, T) \qquad [5.21]$$

where n_{critical} is the critical value of minor cycles which maximize the crack propagation, n is the number of minor cycles in one loading block, and c_{critical} is the hydrogen concentration

which can saturate the plastic zone in one single cycle. The acceleration factor of minor cycles is a ratio of Eq. [5.21] and Eq. [5.20].

$$\alpha_{\text{acceleration}}(n) = \left[\frac{\ln(1/c_o)}{\ln(\frac{n_{critical}}{nc_{critical}})} \right]^2 \qquad [5.22]$$

Fig. 5.9 shows a linear summation of the crack growth rate of each cycle with the Paris model $\frac{da}{dN} = 2.93E-4*(1-R)^{2.79}$ in one block. Introducing the acceleration factor into this Paris model could predict the crack growth rate in NNpHSCC conditions.

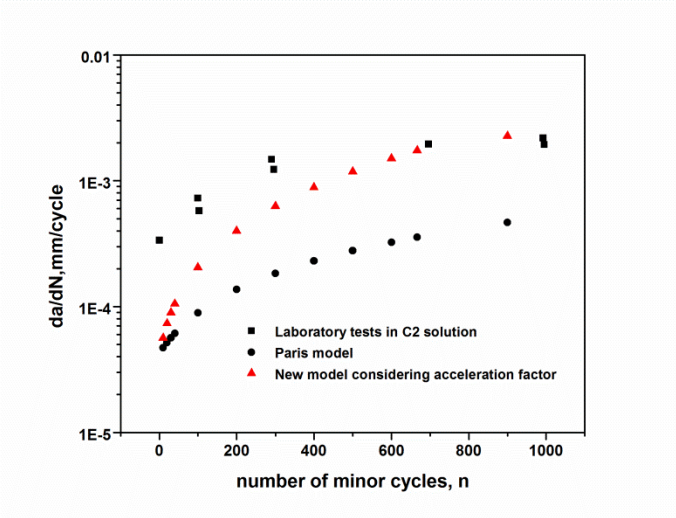

Figure 5.9 The number of minor cycles versus the crack growth rate in one block. The circle symbols are predicted with the original Paris model, the red ones are the predicted values as the acceleration factor was added to the model and the square symbols are the values from the experimental tests.

As Fig. 5.9 shows, although the acceleration factor is considered in assessments, the experimental crack growth rates are larger than the predicted ones, as n is small because the

minor cycles will not only assemble hydrogen atoms but also generate plastic deformations. According to Lynch's theory, the hydrogen atoms can facilitate the linkage of cracks and minor cracks or voids ahead of the crack tip [13,96]. These extra plastic deformations generated from minor cycles had not been considered in previous calculations. For that reason, the difference between the theoretical calculation and laboratory results is reasonable in this case. As n is increased, the difference becomes much smaller. Furthermore, as n reaches the predicted critical value, the predicted crack growth rates are well-matched with the rates from the laboratory tests. The comparison of predicted crack growht rates and experimental results verify the ductile-to-brittle transition which is detected in the laboratory tests. As n is small, the accumulated hydrogen atoms could not saturate the plastic zone and the cracks are ductile. Along with an increase in the number of minor cycles, the cracks become brittle and the crack growth rate would be more dependent on the hydrogen atoms' acceleration effect. In summary, hydrogen diffusion and accumulation in the plastic zone play a decisive role in crack growth.The predicted n_{critical} can be used to quantify the acceleration factor and matches well with laboratory tests.

5.2.3 Conclusion

Hydrogen plays a decisive role in crack growth in NNpHSCC. Hence, the hydrogen acceleration effect should always be quantified in crack growth prediction. The minor cycles' acceleration factor is quantified using MD simulations and experimental works. The follow-up work quantifies the acceleration factor in other loading spectra based on hydrogen accumulation effects. The loading spectrum makes it easier to assemble hydrogen atoms, such as a loading block consisting of minor cycles. Such a loading spectra will always generate a larger crack growth rate.

Chapter VI Conclusions and recommendations

6.1 Conclusions

Our research objective is to enhance our understanding of crack propagation in pipeline steel exposed to near neutral pH under cyclic loading pressure fluctuations. The molecular dynamics simulations are employed in current study. To simplify the problem, a single crystal bcc model is built to simulate the steel, and the dynamic charged method is used to simulate hydrogen accumulation which is induced by pressure fluctuations. The single-static loading is firstly applied to the models with different concentration of hydrogen and different orientations. The results suggest that the crack propagation mechanism is somehow orientation dependent. However, the atomic ratio of H/Fe which leads to brittle cleavage is almost the same for different orientations. Simulations on complicated cyclic loading spectra could be simplified to simulations on constant loading and minor cycles, separately. The crack propagation mechanism in constant cyclic loading could be divided into brittle cleavage and accumulation of hydrogen as dormant crack. Minor cycles accelerate the hydrogen accumulation and reduce the interval between two brittle cleavage statuses. Based on hydrogen accumulation theory and discontinuous crack propagation mechanism, a prediction model of crack growth is developed and validated in our research.

6.1.1 Asymmetric hydrogen diffusion

At low hydrogen concentration, the concentration gradient can be neglected and hydrogen atoms can accumulate into plastic zone because of tensile stress and plastic deformation trapping effects. After hydrogen atoms accumulate into the plastic zone, the concentration

gradient will hinder hydrogen atoms' movement to crack tip, however, tensile stress still provide motivation to accumulate more hydrogen atoms. These competition forces have similar values, but have opposite directions. Hydrogen atoms will continuously accumulate into plastic zone during cyclic loading.

6.1.2 Discontinues crack growth

As hydrogen concentration near crack tip reach a critical value, the crack will become cleavage and propagate rapidly. A small amount of accumulated hydrogen atoms will diffuse out from the free surfaces. Most of the accumulated hydrogen atoms will stay just behind the fracture surface. The crack will become ductile after pass through the hydrogen-rich region. The hydrogen accumulation process will restart again before another brittle cleavage can occur.

6.1.3 Hydrogen accumulation during minor cycles

Minor cycles are cyclic loading with a large R ratio (K_{min}/K_{max}) which is up to 0.9 in our simulations. The nature of these minor cycles is small stress intensity fluctuation. One minor cycle will not contribute to crack propagation (or very small contribution) that offer a stable plastic zone to accumulate hydrogen atoms. The small stress change determines that only a small amount of hydrogen atoms can accumulate into the plastic zone in one minor cycle. In our simulations, we found that hydrogen atoms will increase linearly around crack tip as minor cycles are applied to the models. The linear increment of atomic hydrogen concentration near crack tip help to quantify minor cycles' acceleration factor in underload-minor cycles spectra.

6.1.4 Crack propagation model

Dr. Curtin bridges hydrogen diffusion velocity with crack propagation in a condition which atomic hydrogen exists in bcc structure material (iron). The chemical-potential-determined hydrogen moving velocity affects the velocity where hydrogen rich region forms. As atomic ratio (H/Fe) reaches one ahead of crack tip, the crack will propagate by opening two free surfaces (brittle cleavage). However, hydrogen atoms will saturate the plastic zone before saturate the crack tip. Hence the number of hydrogen atoms saturate the plastic zone should also be considered into determining crack growth rate. Based on this hypothesis, a model that involves in hydrogen diffusivity, stress intensity fluctuations, pH changes, and temperature changes has been developed to quantify crack growth.

6.1.5 Modification of model

The model is based on hydrogen diffusion and could be used to predict crack propagation. This model has successfully predicted critical loading frequency in constant cyclic loading and the number of minor cycles which maximize crack growth in underload spectra. A comparison of this model with classical model (Paris law) has verified its predictive capability in crack growth. The correlation with the combined factor which is developed by Dr. Chen has proved that this model has considered loading frequency and critical loading frequency value. This model could be further modified to predict the minor cycles' acceleration factor to underload and the crack growth rate of complicate loading spectra such as under-overload cycles.

6.2 Recommendation

1. The improvement of the accuracy of prediction involves in accurate diffusivity (D) in steel, and quantifying the relation of hydrogen concentration with temperature. The fitting parameter in the model should be determined separately in different steels. Since crack growth is not only related to hydrogen concentration but pressure fluctuations, the acceleration factor or retardation factor in different spectra should also be determined separately.

2. The semi-brittle theory has illustrated ductile to brittle transition as a process trans-granular cracking change to inter-granular cracking. The grain boundaries in steel will hinder dislocation movement which will increase the local strain energy and make the inter-granular cracking occur. Hydrogen atoms will accumulate near grain boundaries because of trapping effects of grain boundaries. Hydrogen atoms could further change the grain boundaries' ability in hindering dislocation motion and in this way enhance brittle cleavage. This effect is somehow related to grain boundary energy change and awaits to be quantified.

Reference

[1] W.H. Johnson, Proc. R. Soc. London 23 (1874) 168–179.

[2] J. a. Beavers, B. a. Harle, J. Offshore Mech. Arct. Eng. 123 (2001) 147.

[3] M. Yu, W. Chen, R. Kania, G. Van Boven, J. Been, IPC2014 (2014) 1–10.

[4] J.P. Thomas, R.P. Wei, Mater. Sci. Eng. A 159 (1992) 205–221.

[5] S. Wang, W. Chen, F. King, T. Jack, R. Fessler, Corrosion (2002) 526–534.

[6] I.M. Robertson, P. Sofronis, a. Nagao, M.L. Martin, S. Wang, D.W. Gross, K.E. Nygren, Metall. Mater. Trans. A 46 (2015) 2323–2341.

[7] Y. Murakami, T. Kanezaki, P. Sofronis, Eng. Fract. Mech. 97 (2013) 227–243.

[8] R.A. Oriani, P.H. Josephic, Acta Metall. 22 (1974) 1065–1074.

[9] A.R. Troiano, Trans. ASM 52 (1960) 54–80.

[10] N.J. Petch, P. Stables, Nature (1952) 842–843.

[11] M. Koyama, C.C. Tasan, E. Akiyama, K. Tsuzaki, D. Raabe, Acta Mater. 70 (2014) 174–187.

[12] W. Chen, R. Kania, R. Worthingham, G. Van Boven, Acta Mater. 57 (2009) 6200–6214.

[13] S.P. Lynch, Scr. Mater. 65 (2011) 851–854.

[14] D. Tromans, Acta Metall. Mater. 42 (1994) 2043–2049.

[15] I.M. Robertson, H.K. Birnbaum, Hydrogen Effects on Plasticity, Elsevier, 2009.

[16] E. Hayward, C.-C. Fu, Phys. Rev. B 87 (2013) 174103.

[17] R. Oriani, Mill Rd. Gd. Ave, Park Ridge, New Jersey 7656, USA, (1985) 886.

[18] R.A. Cottis, Shreir's Corros. 2 (2010) 902–922.

[19] S.P. Lynch, Scr. Metall. 13 (1979) 1051–1056.

[20] H.K. Birnbaum, P. Sofronis, Mater. Sci. Eng. A 176 (1994) 191–202.

[21] M.S. Daw, M.I. Baskes, Phys. Rev. Lett. 50 (1983) 285–288.

[22] J. Song, W. a. Curtin, Acta Mater. 68 (2014) 61–69.

[23] S. Wang, M.L. Martin, P. Sofronis, S. Ohnuki, N. Hashimoto, I.M. Robertson, Acta Mater. 69 (2014) 275–282.

[24] S. Gahr, M.L. Grossbeck, H.K. Birnbaum, Acta Metall. 25 (1977) 125–134.

[25] D.S. Shih, I.M. Robertson, H.K. Birnbaum, Acta Metall. 36 (1988) 111–124.

[26] I.M. Robertson, P. Sofronis, A. Nagao, M.L. Martin, S. Wang, D.W. Gross, K.E. Nygren, Metall. Mater. Trans. B 46 (2015) 1085–1103.

[27] a Van der Ven, Acta Mater. 52 (2004) 1223–1235.

[28] J. Song, W. a. Curtin, Acta Mater. 59 (2011) 1557–1569.

[29] J. Song, W. a Curtin, Nat. Mater. 12 (2013) 145–51.

[30] Y. Kang, W. Chen, R. Kania, G. Van Boven, R. Worthingham, Corros. Sci. 53 (2011) 968–975.

[31] M. Yu, W. Chen, R. Kania, G. Van Boven, J. Been, Int. J. Fatigue 82 (2016) 658–666.

[32] M. Yu, X. Xing, H. Zhang, J. Zhao, R. Eadie, W. Chen, J. Been, G. Van Boven, R. Kania, Acta Mater. 96 (2015) 159–169.

[33] W. Chen, R.L. Sutherby, Metall. Mater. Trans. A 38 (2007) 1260–1268.

[34] G.A. Mansoori, J.M. Haile, Am. Chem. Soc. 204 (1983) 73–106.

[35] B.J. Alder, T.E. Wainwright, J. Chem. Phys. 27 (1957) 1208–1209.

[36] J.B. Gibson, A.N. Goland, M. Milgram, G.H. Vineyard, Phys. Rev. 120 (1960) 1229–1253.

[37] A. Rahman, F.H.J. Stillinger, J. Chem. Phys. 55 (1971) 3336–3359.

[38] Y. Fukai, J. Less-Common Met. 101 (1984) 50.

[39] D.E. Jiang, E.A. Carter, Phys. Rev. B - Condens. Matter Mater. Phys. 70 (2004) 1–9.

[40] R. Matsumoto, S. Taketomi, S. Matsumoto, N. Miyazaki, Int. J. Hydrogen Energy 34 (2009) 9576–9584.

[41] S.J. Fensin, S.M. Valone, E.K. Cerreta, G.T.G. Iii, 083529 (2012) 1–6.

[42] M. Yuasa, D. Nishihara, M. Mabuchi, Y. Chino, J. Phys. Condens. Matter (2012).

[43] M. Wen, Z. Li, A. Barnoush, Adv. Eng. Mater. 15 (2013) 1146–1151.

[44] K.N. Solanki, D.K. Ward, D.J. Bammann, Metall. Mater. Trans. A 42 (2010) 340–347.

[45] C. Moriconi, G. Hénaff, D. Halm, Int. J. Fatigue 68 (2014) 56–66.

[46] X. Tong, H. Zhang, D.Y. Li, Sci. Rep. 5 (2015) 8459.

[47] A. Latapie, D. Farkas, Phys. Rev. B 69 (2004) 134110.

[48] X. Liu, W. Xie, W. Chen, H. Zhang, J. Mater. Res. 26 (2011) 2735–2743.

[49] W. Beck, J.O. Bockris, J. McBreen, L. Nanis, Proc. R. Soc. A Math. Phys. Eng. Sci. 290 (1966) 220–235.

[50] H. Haftbaradaran, J. Song, W. a. Curtin, H. Gao, J. Power Sources 196 (2011) 361–370.

[51] J. Song, M. Soare, W. a Curtin, Model. Simul. Mater. Sci. Eng. 18 (2010) 045003.

[52] K. Nishimura, N. Miyazaki, Comput. Mater. Sci. 31 (2004) 269–278.

[53] L. Ma, S. Xiao, H. Deng, W. Hu, Int. J. Fatigue 68 (2014) 253–259.

[54] M. Parrinello, A. Rahman, R. a. Parrinello M, Phys. Rev. Lett. 45 (1980) 1196–1199.

[55] S.M. Foiles, M.I. Baskes, M.S. Daw, Phys. Rev. B 33 (1986) 7983–7991.

[56] H. Horner, Zeitschrift Ffir Phys. 89 (1967) 72–89.

[57] W.W. Wood, Nuovo Cim. 9 (1958) 133–143.

[58] H. Chamati, N.I. Papanicolaou, Y. Mishin, D.A. Papaconstantopoulos, Surf. Sci. 600 (2006) 1793–1803.

[59] A. Ramasubramaniam, M. Itakura, E. a. Carter, Phys. Rev. B 79 (2009) 174101.

[60] M.I. Mendelev, S. Han, D.J. Srolovitz, G.J. Ackland, D.Y. Sun, M. Asta, Philos. Mag. 83 (2003) 3977–3994.

[61] A. Beste, J. Phys. Chem. A 118 (2014) 803–814.

[62] T.C.O. Connor, J. Andzelm, M.O. Robbins, J. Chem. Phys. 142 (2015).

[63] C. Lee, B. Lukose, M.O. Thompson, P. Clancy, Phys. Rev. B 91 (2015).

[64] H. Grubmüller, H. Heller, a. Windemuth, K. Schulten, Mol. Simul. 6 (1991) 121–142.

[65] R.E. Gillilan, K.R. Wilson, J. Chem. Phys. 97 (1992) 1757.

[66] B.J. Palmer, J. Comput. Phys. 104 (1993) 470–472.

[67] W.F. Van Gunsteren, H.J.C. Berendsen, Mol. Simul. 1 (1988) 173–185.

[68] K. Diethelm, N. Ford, A. Freed, Nonlinear Dyn. (2002) 3–22.

[69] D.J.E. Callaway, A. Rahman, Phys. Rev. Lett. 49 (1982) 613–616.

[70] D.J. Evans, B.L. Holian, J. Chem. Phys. 83 (1985) 4069–4074.

[71] R.C. Pond, V. Vitek, Proc. R. Soc. London (1977) 453–470.

[72] E.R. Smith, I.K. Snook, W. Van Megen, Phys. A Stat. Mech. Its Appl. 143 (1987) 441–467.

[73] M. Alves, N. Jones, J. Mech. Phys. Solids 47 (1999) 643–667.

[74] T.L. Anderson, Fracture Mechanics, Fundermentals and Applications, 3rd ed., 2005.

[75] D.J. Dever, J. Appl. Phys. 43 (1972) 3293.

[76] W. Xie, X. Liu, W. Chen, H. Zhang, Comput. Mater. Sci. 50 (2011) 3397–3402.

[77] C.D. Beachem, Metall. Trans. 3 (1972) 441–455.

[78] I. Scheider, M. Pfuff, W. Dietzel, Eng. Fract. Mech. 75 (2008) 4283–4291.

[79] V. Olden, A. Alvaro, O.M. Akselsen, Int. J. Hydrogen Energy 37 (2012) 11474–11486.

[80] E. Hornlund, J.K.T. Fossen, S. Hauger, C. Haugen, T. Havn, T. Hemmingsen, Int. J. Electrochem. Sci. 2 (2007) 82–92.

[81] R.A. Oriani, Acta Metall. 18 (1970) 147–157.

[82] J. Von Pezold, L. Lymperakis, 59 (2011) 2969–2980.

[83] P. Taylor, J. Barton, A.C.F. Cocks, Philos. Mag. 93 (2013) 37–41.

[84] Y. Kang, W. Chen, R. Kania, G. Van Boven, R. Worthingham, Corros. Sci. 53 (2011) 968–975.

[85] M. Yu, W. Chen, R. Kania, G. Van Boven, J. Been, Fatigue Fract. Eng. Mater. Struct. 38 (2015) 681–692.

[86] N. Metropolis, A.W. Rosenbluth, M.N. Rosenbluth, A.H. Teller, E. Teller, J. Chem. Phys. 21 (1953) 1087.

[87] S. Pieprzyk, D.M. Heyes, S. Maćkowiak, a C. Brańka, Phys. Rev. E. Stat. Nonlin. Soft Matter Phys. 91 (2015) 033312.

[88] W.G. Hoover, B. Lee, Phys. Lett. A 211 (1996) 253–257.

[89] M. Daw, M. Baskes, Phys. Rev. B 29 (1984).

[90] Steve Plimton, J. Comput. Phys. 117 (1995) 1–19.

[91] S. Taketomi, R. Matsumoto, N. Miyazaki, Acta Mater. 56 (2008) 3761–3769.

[92] D.H. Warner, W. a. Curtin, Acta Mater. 57 (2009) 4267–4277.

[93] D.H. Warner, W. a Curtin, S. Qu, Nat. Mater. 6 (2007) 876–81.

[94] D.E. Jiang, E. a. Carter, Acta Mater. 52 (2004) 4801–4807.

[95] S.B. Gesari, B.L. Irigoyen, A. Juan, Rev. Lit. Arts Am. 12 (2005) 227–232.

[96] Y. Murakami, T. Kanezaki, Y. Mine, Metall. Mater. Trans. A 41 (2010) 2548–2562.

[97] X. Xing, W. Chen, H. Zhang, Mater. Lett. 152 (2015) 86–89.

[98] C. Reuber, P. Eisenlohr, F. Roters, D. Raabe, Acta Mater. 71 (2014) 333–348.

[99] M. Meisnar, A. Vilalta-clemente, M. Moody, K. Arioka, S. Lozano-perez, Acta Mater. 114 (2016) 15–24.

[100] M.L. Martin, P. Sofronis, I.M. Robertson, T. Awane, Y. Murakami, Int. J. Fatigue 57 (2013) 28–36.

[101] I.M. Dmytrakh, O.D. Smiyan, a. M. Syrotyuk, O.L. Bilyy, Int. J. Fatigue 50 (2013) 26–32.

[102] Z.Y. Liu, X.G. Li, Y.F. Cheng, Corros. Sci. 55 (2012) 54–60.

[103] S. Benbelaid, M. a. Belouchrani, Y. Assoul, B. Bezzazi, Int. J. Damage Mech. 20 (2010) 831–844.

[104] E.V. Chatzidouros, V.J. Papazoglou, T.E. Tsiourva, D.I. Pantelis, Int. J. Hydrogen Energy 36 (2011) 12626–12643.

[105] T.N.O. Industrie, A.M. Apeldoorn, S. International, O. Products, C.M. Amsterdam, J. Mech. Phys. Solids 47 (1999) 860–881.

[106] L. Vergani, C. Colombo, G. Gobbi, F.M. Bolzoni, G. Fumagalli, Procedia Eng. 74 (2014) 468–471.

[107] M. Dadfarnia, P. Novak, D.C. Ahn, J.B. Liu, P. Sofronis, D.D. Johnson, I.M. Robertson, Adv. Mater. 22 (2010) 1128–35.

[108] H. Momida, Y. Asari, Y. Nakamura, Y. Tateyama, T. Ohno, Phys. Rev. B 88 (2013) 144107.

[109] T. Doshida, M. Nakamura, H. Saito, T. Sawada, K. Takai, Acta Mater. 61 (2013) 7755–7766.

[110] M.D. Sangid, T. Ezaz, H. Sehitoglu, I.M. Robertson, Acta Mater. 59 (2011) 283–296.

[111] Y. Shibuta, K. Oguchi, T. Suzuki, ISIJ Int. 52 (2012) 2205–2209.

[112] T. Doshida, K. Takai, Acta Mater. 79 (2014) 93–107.

[113] M. Skorupa, Fatigue Fract. Eng. Mater. Struct. 22 (1999) 905–926.

[114] W.-P. Wu, Y.-L. Li, X.-Y. Sun, Comput. Mater. Sci. 109 (2015) 66–75.

[115] A.M. Syrotyuk, I.M. Dmytrakh, Mater. Sci. 50 (2015) 475–487.

[116] X. Xing, M. Yu, W. Chen, H. Zhang, Comput. Mater. Sci. (n.d.).

[117] H. Kanayama, M. Ogino, R. Miresmaeili, T. Nakagawa, T. Toda, J. Comput. Sci. Technol. 2 (2008) 499–510.

[118] K. Kawamoto, Y. Oda, H. Noguchi, H. Fujii, T. Izumi, G. Itoh, J. Solid Mech. Mater. Eng. 3 (2009) 898–909.

[119] C.D. Beachem, Metall. Trans. 3 (1972) 441–455.

[120] J.E. Angelo, N.R. Moody, M.I. Baskes, X. Sha, Model. Simul. Mater. Sci. Eng. 5 (1997) 651–652.

[121] A. Barnoush, H. Vehoff, Acta Mater. 58 (2010) 5274–5285.

[122] W. Gerberich, H. Huang, Metall. Trans. … 24 (1993) 535–543.

[123] R. Kania, R. Worthingham, in:, 2015, pp. 1–8.

[124] M. Kelestemur, T. Chaki, Fatigue Fract. Eng. Mater. Struct. 24 (2001) 15–22.

[125] M. Skorupa, Fatigue Fract. Eng. Mater. Struct. 21 (1998) 987–1006.

[126] P.S. Song, Y.L. Shieh, Eng. Fract. Mech. 71 (2004) 1577–1584.

[127] A. Vasudeven, K. Sadananda, N. Louat, Mater. Sci. Eng. A 188 (1994) 1–22.

[128] J. Been, R. Eadie, R. Sutherby, IPC2006-10345 , Proc. IPC 2006 Int. Pipeline Conf., 2006.

Appendix

Calculation of hydrogen-moving rate

Chemical potential driven hydrogen diffusion is expressed by Eq. (1) [28]

$$\mu = \mu_o + k_B T \ln \frac{c}{1-c} + \sigma^{hyd} \Omega \tag{1}$$

where μ_o is constant and the meaning of other parameters can be checked in the manuscript. And the axial hydrogen moving rate is shown as Eq. (2)

$$V_r = \frac{DF_r}{k_B T}, F_r = -\left(\nabla \mu\right)_r \tag{2}$$

and the stress distribution related moving rate Vr^{σ} is expressed as Eq. (3) [29]

$$V_r^{\sigma} = -\frac{D\Omega}{k_B T}\left(\nabla \sigma^{hyd}\right)_r, \frac{\partial \sigma^{hyd}}{\partial r} = -\frac{\left(1+\nu\right)K_I}{3\sqrt{2\pi} r^{3/2}} \cos\left(\tfrac{\theta}{2}\right) \tag{3}$$

and the hydrogen concentration gradient related moving rate as the hydrogen concentration reach equilibrium is expressed as,

$$V_r^c = -D\left(\nabla \ln\left(\frac{c_{eq}}{1-c_{eq}}\right)\right)_r = \frac{-D}{c_{eq}\left(1-c_{eq}\right)}\left(\nabla c_{eq}\right)_r,$$

$$\frac{\partial c_{eq}}{\partial r} = -c_{eq}\frac{\Omega}{k_B T}\frac{\left(1+\nu\right)K_I}{3\sqrt{2\pi} r^{3/2}} \cos\left(\frac{\theta}{2}\right) \tag{4}$$

Calculation the value of accumulated hydrogen atoms

There is another method to calculate the number of hydrogen atoms required to saturate the plastic zone. Under experimental condition, for a max stress intensity, K_{max}=33MPa*$m^{0.5}$,

R=0.5, and in X-65 steel, the critical loading frequency corresponding to the loading condition is 10^{-3}Hz and the critical loading time, $t_{critical} = 1/2f_{critical}$, of one cycle is 500s [32].

$$f_{critical} = \frac{(1+v)\Omega D(K_{max}+K_{min})\left(\frac{1}{\sqrt{r_p}}-\frac{1}{\sqrt{R_{eq}}}\right)}{\pi\left(R_{eq}-r_p\right)^2 k_B T 3\sqrt{2\pi}} \quad (5)$$

Critical loading frequency is corresponding to the minimum time that hydrogen atoms require to diffuse and reach momentum equilibrium in the plastic zone. If c_o is increased, the number of hydrogen atoms required to achieve the equilibriun is increased. And if c_o could further increase to the critical value $c_{critical}$, the plastic zone can the saturated and the crack growth rate should be maximized.

Hence, as the loading time is larger than $t_{critical}$, the crack propagation rate will reach a maximum and remain constant [32]. The number of hydrogen atoms required to saturate the plastic zone and allow for DTB transition to occur is

$$N_H^{total} = \frac{c_{critical} l_z \left[\pi\left(r_p + \overline{V_r} * t_{critical}\right)^2 - \pi r_p^2\right]}{a_o^3/2} \quad (6)$$

where $c_{critical}$ is the theoretical value, which is previously determined to be equal to 280ppm, $t_{critical}$ is the loading time corresponding to the critical loading frequency, l_z is the thickness of the specimen, and $\overline{V_r}$ is the average hydrogen-movement velocity at the boundary of the plastic zone.

This calculation based on the same assumptions as calculating hydrogen atoms accumulate into the plastic zone in each minor cycle. The diffusivity of hydrogen atoms outside the plastic zone is assumed to be constant since these regions are not stress concentrated. As the

stress intensity changes from K_{min} to K_{max} in a range of time t, the hydrogen atoms can diffuse into the plastic zone from a farthest position $r_P+\bar{V}_r*t$. The total volume of the annulus red region in Fig. 2.2 which offers hydrogen atoms to the plastic zone during loading can be estimated as $l_z[\pi(r_p+\bar{V}_r*t)^2-\pi r_p^2]$. There are not a lot plastic deformations outside the plastic zone, hence the red region is assumed to be in bcc structure. And the total number of Fe atoms contained in the red region is $l_z[\pi(r_p+\bar{V}_r*t)^2-\pi r_p^2]/(a_o^3/2)$, where $a_o^3/2$ is the volume taken by each Fe atom. If the atomic ratio of H/Fe reached the critical value and the diffusion time was bigger than $t_{critical}$, the plastic zone can be saturated and the number of H atoms required is calculated with Eq. (2). Hence, the predicted value of minor cycles required to make the ductile-to-brittle transition occur is equal to $\frac{N_H^{total}}{N_H^{minorcycle}}$, or 676 cycles. This value is consistant with the critical number, which the value of hydrogen atoms is calculated according to hydrostatic stress and dislocation stress distribution. The assessment process verifies the hydrogen accumulation theory.